Transactions of Tianjin University (2022) 28:265–291
https://doi.org/10.1007/s12209-022-00330-1

REVIEW

Rational Manipulation of Intermediates on Copper for CO_2 Electroreduction Toward Multicarbon Products

Guangyi Jiang[1,2,3] · Daliang Han[1,2,3] · Zishan Han[1,2,3] · Jiachen Gao[1,2,3] · Xinyu Wang[1,2,3] · Zhe Weng[1,2,3] · Quan-Hong Yang[1,2,3,4]

Received: 12 May 2022 / Revised: 14 June 2022 / Accepted: 29 June 2022 / Published online: 3 August 2022

Abstract

Excess greenhouse gas emissions, primarily carbon dioxide (CO_2), have caused major environmental concerns worldwide. The electroreduction of CO_2 into valuable chemicals using renewable energy is an ecofriendly approach to achieve carbon neutrality. In this regard, copper (Cu) has attracted considerable attention as the only known metallic catalyst available for converting CO_2 to high-value multicarbon (C_{2+}) products. The production of C_{2+} involves complicated C–C coupling steps and thus imposes high demands on intermediate regulation. In this review, we discuss multiple strategies for modulating intermediates to facilitate C_{2+} formation on Cu-based catalysts. Furthermore, several sophisticated in situ characterization techniques are outlined for elucidating the mechanism of C–C coupling. Lastly, the challenges and future directions of CO_2 electroreduction to C_{2+} are envisioned.

Keywords CO_2 electroreduction · Copper-based electrocatalysts · Multicarbon products · Intermediate · C–C coupling

Introduction

Massive carbon dioxide (CO_2) emissions arising from industrial activities have caused a substantial increase in the atmospheric CO_2 concentration, and the ensuing global warming has resulted in increasingly frequent environmental disasters such as starvation, habitat loss, species extinction, and sea-level rise [1, 2]. To tackle these problems, carbon capture, utilization, and storage have been conceived as pathways to peak carbon emissions and eventually reach a carbon–neutral society before 2060 [3]. Electrochemical CO_2 reduction reaction (CO_2RR) powered by renewable electricity provides a sustainable solution for converting waste CO_2 emissions into useful feedstocks and thereby realizing a net negative carbon footprint and long-term storage of the intermittent renewable electricity in chemical bonds [4, 5]. In the past three decades, significant progress has been achieved in using CO_2RR to generate diverse products, including CO [6–9], HCOOH [10, 11], CH_4 [12–14], C_2H_4 [15–17], C_2H_5OH [18–20], and n-C_3H_7OH [21–23]. Compared to monocarbon (C_1) products, multicarbon (C_{2+}) products are more desirable because of their higher energy density, richer chemical structure, and more versatile applications [24].

Since CO_2 is a thermodynamically stable molecule with strong C=O bonds (750 kJ/ mol) [25], converting CO_2 to C_{2+} products is extremely difficult. Copper (Cu) is the only known metallic electrocatalyst capable of generating C_{2+} products in considerable amounts [26–28]. However, its selectivity and the activity of the C_{2+} products are drastically limited by the sluggish kinetics of the C–C coupling step (i.e., the bifurcation for the generation of C_{2+} and C_1 products), as well as because of competition with H–H formation [29]. In the multielectron and multiproton transfer process of CO_2RR, the adsorption energy and coverage of key intermediates, such as *H, *COOH, *OCHO, and *CO, are commonly considered

Guangyi Jiang and Daliang Han are equal major contributors.

✉ Zhe Weng
zweng@tju.edu.cn

1 Nanoyang Group, State Key Laboratory of Chemical Engineering, School of Chemical Engineering and Technology, Tianjin University, Tianjin 300072, China

2 Haihe Laboratory of Sustainable Chemical Transformations, Tianjin 300192, China

3 Collaborative Innovation Center of Chemical Science and Engineering (Tianjin), Tianjin 300072, China

4 Joint School of National University of Singapore and Tianjin University, International Campus of Tianjin University, Binhai New City, Fuzhou 350207, China

to determine the reaction routes and activity of CO_2RR [30, 31]. For example, the first proton-coupled transfer reaction will generate *OOCH or *COOH intermediates. *OOCH is the intermediate for formate production, while *COOH is the intermediate for the formation of CO gas or *CO, which is a key intermediate for C–C coupling [32, 33]. Theoretical calculations indicate that the binding energy of *H weakens with increasing *CO coverages, and this in turn inhibits the activity of the competing hydrogen evolution reaction (HER) [31]. Therefore, controlling the intermediate adsorption is critical for inhibiting the formation of H_2 and C_1 products but facilitating the formation of adsorbed CO dimers (e.g., *CO–CO or *CO–CHO). In addition, Cu moderately binds with most intermediates, resulting in multiple reaction pathways and thus yielding a mixture of numerous products [26]. To improve the selectivity and activity of C_{2+} products, a variety of strategies such as grain boundary exposure [34–36], heteroatom doping [37, 38], and local microenvironment regulation [39, 40] were developed to manipulate the adsorption state of intermediates and facilitate their deep reduction.

This review focuses on integrated strategies for regulating the adsorption state of intermediates and their influence on C_{2+} production for Cu-based electrocatalysts (Fig. 1). Moreover, we discuss the vital role of in situ characterization techniques for examining CO_2RR intermediates. Finally, we highlight the challenges and perspectives associated with the electroreduction of CO_2 to C_{2+} products. This review can provide a better understanding of the principles of catalyst design with the aim of achieving an overall improvement for the CO_2-to-C_{2+} catalytic systems.

Proposed Mechanisms for CO_2RR Toward C_{2+} Products

Since Hori et al. [41, 42] first discovered that Cu is capable of electroreducing CO_2 to C_{2+} products, Cu-based catalysts have been recognized as the best electrocatalysts for C_{2+} production during the past three decades. To investigate the origin of the deep reduction activity of Cu, the binding energies of the adsorbed CO (*CO) and hydrogen (*H) were used as a descriptor to predict the CO_2RR product distribution of different metal catalysts [26, 43]. In the case of metals such as Au and Ag that bind weakly to *CO and *H, *CO prefers direct desorption to form CO. Metals such as Pt and Fe have high binding strength with *CO, but their favorable adsorption of *H facilitates HER. Unlike in the case of those metals, the adsorption energy of *CO and *H

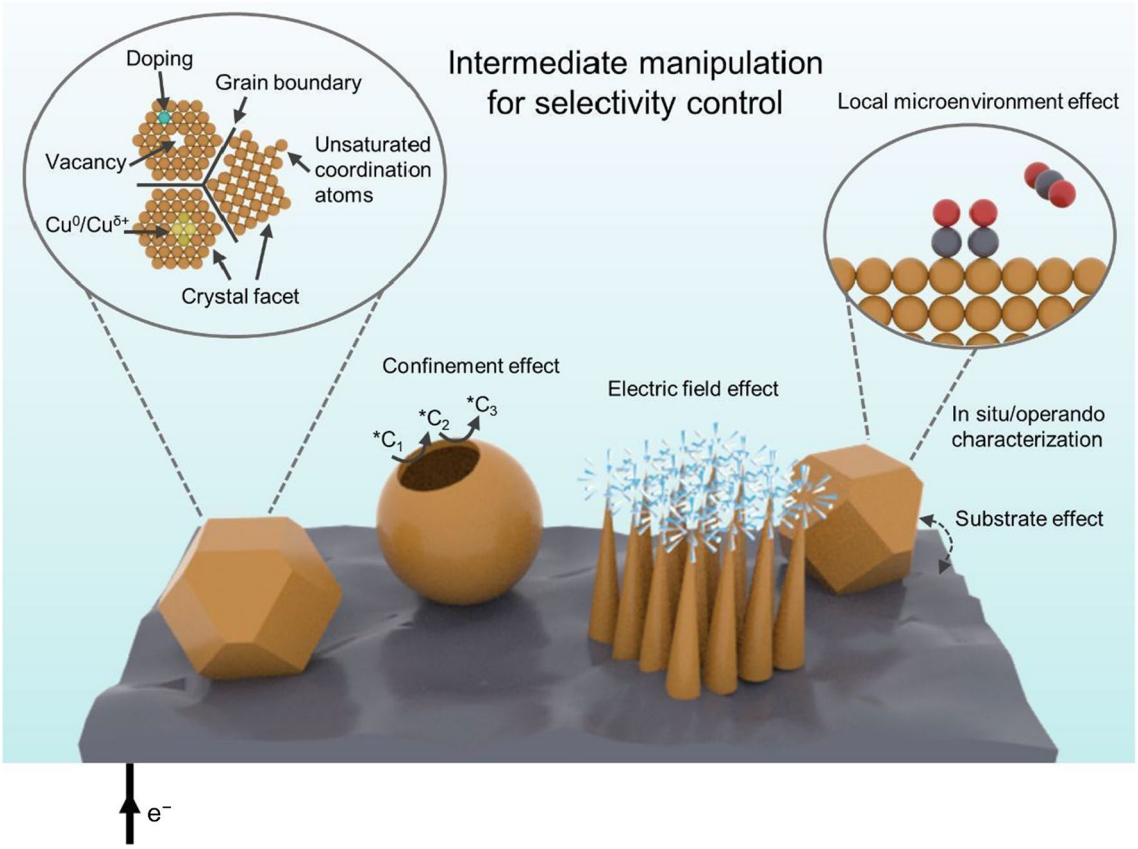

Fig. 1 Schematic illustration of the intermediate manipulation strategies for the electrochemical CO_2 reduction reaction (CO_2RR) toward multicarbon products

on Cu is neither too strong to poison its active sites nor too weak to be immediately desorbed. This moderate intermediate binding energy of Cu enables continuous C–C coupling and multistep hydrogenation, which is essential for the deep reduction of CO_2 beyond CO.

Different reaction routes have been proposed for C_{2+} formation (Fig. 2). *CO is generally recognized as a key reaction intermediate in the electroreduction of CO_2 to C_{2+} products [29, 44, 45]. The dimerization of *CO [46, 47] and coupling of *CO with protonated *CO (*CHO or *COH) [48, 49] are widely accepted possible routes for C–C coupling. In the *CO dimerization mechanism, C–C coupling is generally regarded as the rate-determining step (RDS) for C_{2+} production and has been widely applied in theoretical calculations [50, 51]. In this case, two *CO intermediates on the Cu surface are coupled to form *OCCO, and this process is accompanied by an electron transfer [52]. However, density functional theory (DFT) simulations suggest that the RDS of C_{2+} products may be changed from *CO dimerization to *CO–*CHO or *CO–*COH coupling with the increase in the local *CO coverage at higher negative potentials [53]. In the mechanism of *CO coupling with hydrogenated *CO, *CO hydrogenation is considered the RDS for C_{2+} formation on Cu (111) and (100) surfaces [54]. The competition between *CO and proton sources (i.e., *H, H^+, or adsorbed H_2O) on the active sites of Cu will lead to a shift

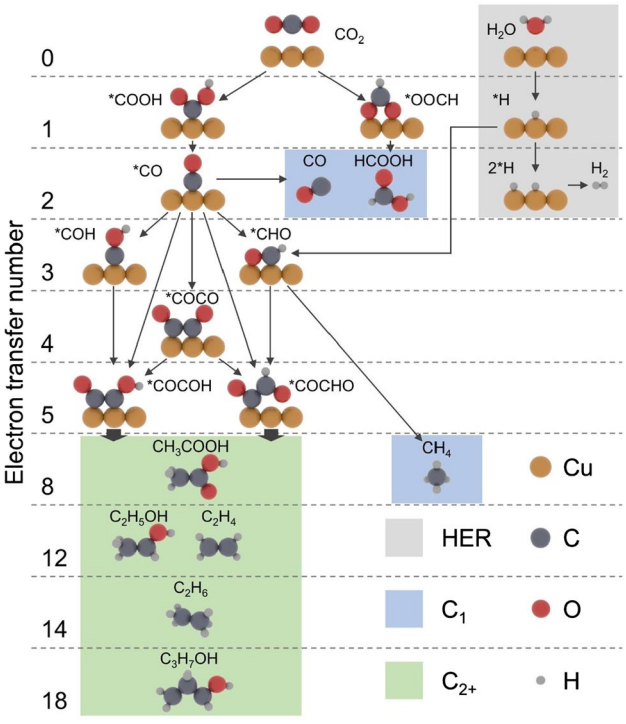

Fig. 2 Possible reaction routes for the electrochemical CO_2RR toward multicarbon products

in product distribution [55, 56]. After the C–C coupling step, the *COCHO or *COCOH is subsequently reduced to *CHCOH, which is a common precursor of C_2H_4 and C_2H_5OH [57, 58]. *CHCOH deoxygenation to *CCH or hydrogenation to *CHCHOH can generate C_2H_4 and C_2H_5OH, respectively [20].

In addition, the formation of C_3 products on Cu has been observed. Some rationally designed Cu catalysts attained a Faradaic efficiency (FE) of up to 15.4% for *n*-propanol (the major C_3 product) in CO_2RR (33% in CO reduction reaction (CORR)) [21, 59]. However, the reaction pathway to C_3 products, which inevitably requires two successive C–C coupling steps, has not been well-studied yet because of the lack of sophisticated characterization techniques for $*C_{2+}$ intermediates. As an approximate solution, electroreducing C_2/C_3 compounds toward those C_3 products that may share the reaction pathway as the electrochemical CO_2RR toward the same products is employed for a preliminary mechanistic exploration. Hori et al. [60] found that the electroreduction of propionaldehyde produces large amounts of *n*-propanol, suggesting that propionaldehyde is a potential intermediate for the *n*-propanol product. Through electrochemical differential mass spectrometry, Bell's group [61] observed that the relative abundance of ethanol increased at the expense of propionaldehyde at more cathodic potentials. This observation indicates that ethanol and propionaldehyde share the same intermediate ($*CH_3CHO$). To identify the intermediates for the second C–C coupling step, Zhang et al. [62] performed a co-electroreduction of isotopically labeled CO and acetaldehyde and found that only a minor fraction (up to 36%) of the *n*-propanol product originates from the cross-coupling between CO and acetaldehyde. The adsorbed methylcarbonyl ($*OCH_2CH_3$ or $*CHOHCH_3$) is considered a possible intermediate for the second C–C coupling step, in which the reaction pathways bifurcate toward C_2 or C_3 products. Therefore, a reasonable speculation for the C_3 pathway is that a $*C_2$ intermediate undergoes intermolecular C–C coupling with a neighboring *CO intermediate, and this is followed by proton or electron transfer to form propionaldehyde. The key to C_3 production is to stabilize $*C_2$ intermediates and optimize the *CO coverage [22, 63].

In conclusion, the C–C coupling step is essential for the conversion of CO_2 to C_{2+} products. This step is regulated by the adsorption states of the intermediates on Cu. With regard to the initial intermediate for C_{2+} generation, the surface coverage and adsorption duration of *CO affect the probability of C–C coupling. Thereafter, the adsorption states of the subsequent intermediates determine the energy barrier of C–C coupling and the followed reaction routes. Thus, manipulating intermediates by rational Cu-based catalyst design is a promising way to produce high-value C_{2+} products efficiently.

Strategies of Intermediate Manipulation for Promoting C_{2+} Production

In the following section, we will summarize the principal strategies of manipulating intermediates, including the surface structural effects, introduction of additional elements, chemical state effects, electric field effects, substrate effects, confinement effects, and local microenvironment effects for promoting the deep conversion of CO_2 to C_{2+} products.

Surface Structural Effects

Crystal Facets

The crystal facet is one of the critical structural parameters for Cu. The adsorption strength of intermediates has a high sensitivity to the crystal facets. Hence, the distributions of CO_2RR products on various crystal facets are different. In general, Cu (111) facets have an appropriate ratio of *CO to *H, and thus, these facets favor CH_4 production. Unlike Cu (111), Cu (100) facets are more favorable for *CO adsorption, thereby promoting C–C coupling to generate C_2H_4 (Fig. 3a, b) [64]. DFT calculations demonstrate that *CO dimerization on Cu (100) exhibits the lowest energy among the low-index Cu facets [49]. Therefore, the selective exposure of Cu (100) facet is an important strategy to improve C_{2+} selectivity [65]. Wang's group [23] selectively exposed Cu (100) facets through the metal-ion battery cycling method, achieving a sixfold improvement in the ratio of C_{2+} and C_1 products compared with the polished Cu foil. Furthermore, the C_{2+}/CH_4 value was plotted as a function of crystal orientation, illustrating that high-index facets can further improve the selectivity for C_{2+} products (Fig. 3c) [42]. For example, Cu (711) is thermodynamically favored for C–C coupling via cross-coupling of the *CO and *COH intermediates based on DFT calculations [66]. Similarly, Cu (751) has higher activity and selectivity for C–C coupling compared to low-index facets [67]. Changes in the Cu facets also affect the activity and selectivity of CO_2RR. High-purity 4H Cu and heterogeneous 4H/ face-centered cubic (fcc) Cu synthesized on the template of 4H and 4H/fcc Au exhibit higher overall activity and catalytic selectivity than fcc Cu, indicating the high dependence of electrocatalytic behaviors on crystal facets (Fig. 3d) [68].

Although the C_{2+} activity and selectivity can be effectively improved by controlling the crystal facet, Cu usually suffers from dynamical reconstruction during the CO_2RR process. This reconstruction causes changes in its original crystal facets and catalytic performance [69, 70]. Besides, note that the active Cu surface may also undergo an irreversible evolution even after the removal of the applied potential [71, 72]. This susceptibility of Cu reconstruction makes it difficult to identify the active sites under realistic conditions [73]. To probe the actual active sites on Cu and to obtain fundamental evidence on structure–activity relationships, numerous in situ characterization techniques have been developed under controlled conditions during CO_2RR [74–76]. Through *operando* electrochemical scanning tunneling microscopy (EC-STM), Kim et al. [77, 78] found that a polycrystalline Cu electrode held at a fixed negative potential undergoes stepwise surface reconstruction in both alkaline and neutral electrolytes, first transforming to Cu (111) and then to Cu (100). The resulting Cu (100) surface remains stable, without further surface transformations, during the subsequent tests. In situ grazing incidence X-ray diffraction (GI-XRD) also revealed the reconstruction of polycrystalline Cu toward the (100) facet in the presence of CO_2 [71]. The degree of reconstruction increases as the applied potential becomes more negative, and the reconstructed facets are partially preserved in the subsequent anodic scanning step. The in situ characterizations described earlier indicate that the dynamic reconstruction of Cu catalysts is mainly driven by the cathode potential, but the influence of adsorbates cannot be ruled out.

Recently, the adsorption of intermediates was shown to affect the formation of preferred crystal facets with high C_{2+} selectivity during the CO_2RR. Wang et al. [79] reported a self-selective method to stabilize the crystal surface with the strongest binding to the target intermediates because the adsorption of reactants tends to reduce the relative surface energies of these surfaces. Sargent's group [80] performed Cu electrodeposition in the presence of CO_2RR intermediates and achieved a 70% increase in the ratio of Cu (100) facets to the total surface area compared to Cu electrodeposited in the presence of HER intermediates (Fig. 3e). This Cu catalyst has a high FE of 90% for the total C_{2+} products at current densities higher than 580 mA/cm^2, and the FE of C_2H_4 remains constant over 65 h of electrolysis. In addition to the reaction intermediates, electrolyte additives also affect the crystal facet reconstruction on Cu catalysts. Our recent work demonstrated that ethylenediamine tetramethylenephosphonic acid (EDTMPA) molecules preferentially adsorb on Cu (110) during the CO_2RR, inducing the selective generation of Cu (110) facets with an intrinsically high *CO binding strength (Fig. 3f, g) [39]. These studies demonstrate that the adsorption of intermediates or electrolyte additives on the catalyst surface can induce the formation of specific crystal facets with high activity; these facets are beneficial for the adsorption and conversion of intermediates.

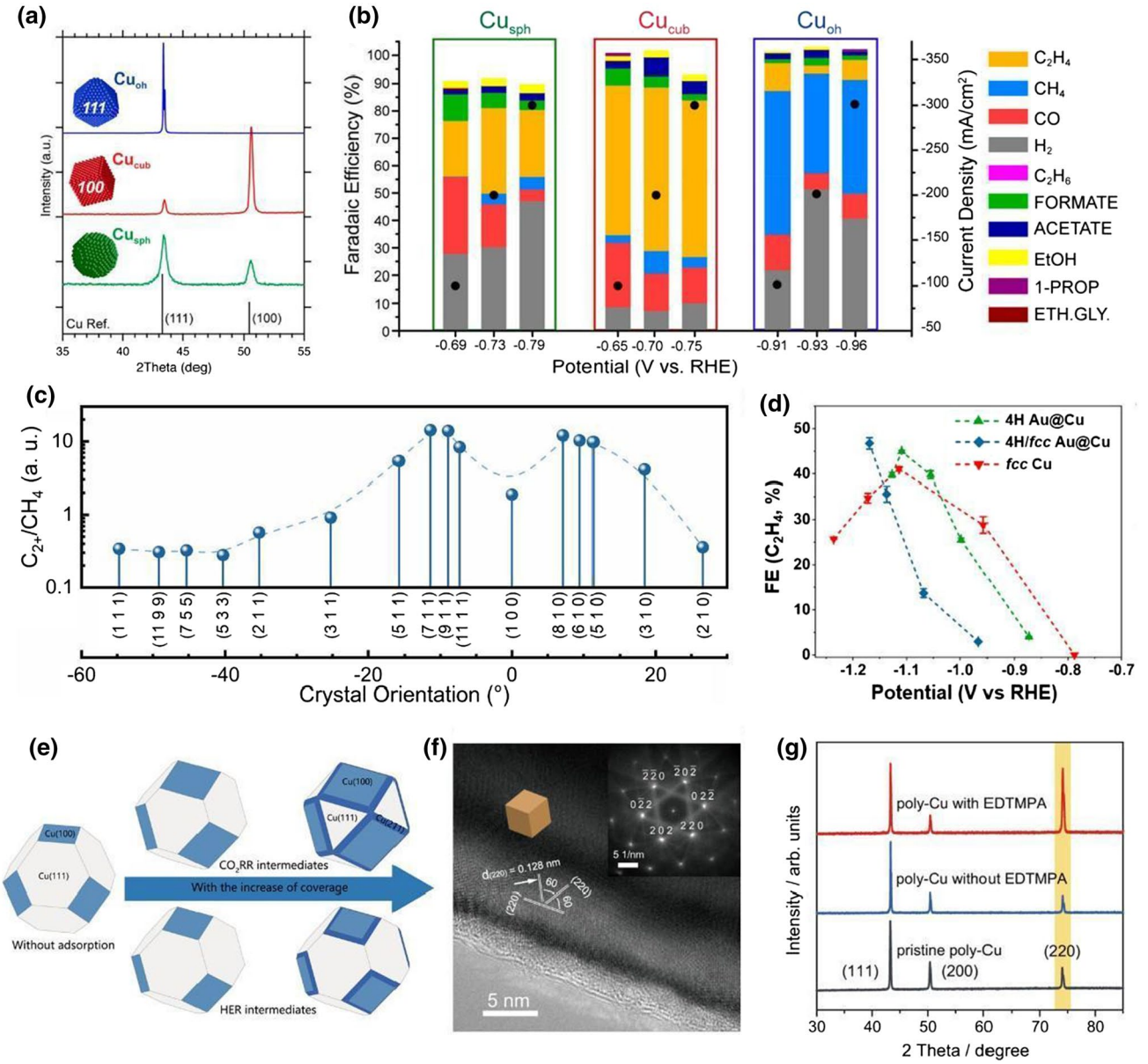

Fig. 3 Improvement of C_{2+} selectivity by crystal facets. **a** X-ray diffraction patterns of Cu octahedra (Cu_{oh}), Cu cubes (Cu_{cub}), and Cu spheres (Cu_{sph}). **b** Selectivity of CO_2RR products on Cu with different facet exposures. Reproduced with permission from Ref. [64]. Copyright 2020 American Chemical Society. **c** Variation in C_{2+}/CH_4 with the angle of the crystal orientation with reference to Cu (100). Reproduced with permission from Ref. [42]. Copyright 2003 Elsevier. **d** Faradic efficiencies (FEs) for producing C_2H_4 on different catalysts. Reproduced with permission from Ref. [68]. Copyright 2020 American Chemical Society. **e** Wulff construction clusters of Cu with the adsorption of CO_2RR or hydrogen evolution reaction (HER) intermediates. Reproduced with permission from Ref. [80]. Copyright 2020 Springer Nature. **f** Transmission electron microscopy (TEM) image of an electrodeposited Cu TEM grid after electrocatalysis in the electrolyte to which ethylenediamine tetramethylenephosphonic acid (EDTMPA) was added. Inset shows the corresponding electron diffraction pattern of the selected area. **g** Grazing incidence X-ray diffraction (GI-XRD) patterns of polycrystalline Cu electrodes before and after electrocatalysis in the electrolytes with and without EDTMPA. Reproduced with permission from Ref. [39]. Copyright 2022 Springer Nature

Unsaturated Coordination Atoms

After obtaining an in-depth understanding of the crystallographic dependence of the product distribution for Cu, the high proportion of unsaturated coordination atoms was also considered to contribute to the high catalytic activity of the high-index crystalline facets for C_{2+} production [67, 81]. CO adsorption energies on low-index Cu facets (i.e., Cu (111), Cu (100), and Cu (110)) and several regular stepped and kinked facets (i.e., Cu (211), Cu (221), and Cu (532)) were

examined by thermal desorption spectroscopy. The results reveal that the high-index crystalline surfaces with a lower coordination number (CN) of surface atoms have higher CO adsorption energies than the low-index ones [82]. In addition to the sites on step edges and joints, the adatoms on the surface also tend to have a higher degree of unsaturation and bind strongly with CO. Theoretical calculations are usually used to reveal the role of adparticles with low CN and surface clusters on the pristine Cu surface in concentrating *CO and facilitating the formation of CO dimers (Fig. 4a–c) [83]. In the presence of Cu adparticles, the reaction barriers between *CO and $*C_2$ intermediates (*OCCOH or $*CCH_2$) are dramatically reduced, enabling the selective electrosynthesis of *n*-propanol. DFT calculations revealed that the highly undercoordinated sites (CN < 5.9) promote C_2H_5OH production; moderate coordination sites (5.9 < CN < 7.5) are beneficial for C_2H_4 production; and high coordination sites (CN > 7.5) have a strong hydrogen adsorption energy [84]. Therefore, the CN of surface catalytic active sites is closely correlated with CO_2RR product selectivity.

The CN of the atoms on the catalyst surface can be adjusted not only by crystal surface control, but also by manipulating the macroscopic morphology. Nanostructuring of the catalyst allows for increasing the specific surface area and exposing more unsaturated coordination atoms, thereby resulting in a low CN catalyst. For example, a high density of undercoordinated Cu was formed on the surface of the Cu foil treated by anodic halogenation and subsequent electroreduction processes, resulting in a selective conversion of CO_2 to C_{2+} products with a FE of 72% [85]. Machine learning was applied to predict the *CO binding energy of 10,433 surface atoms on a rough Cu model, and

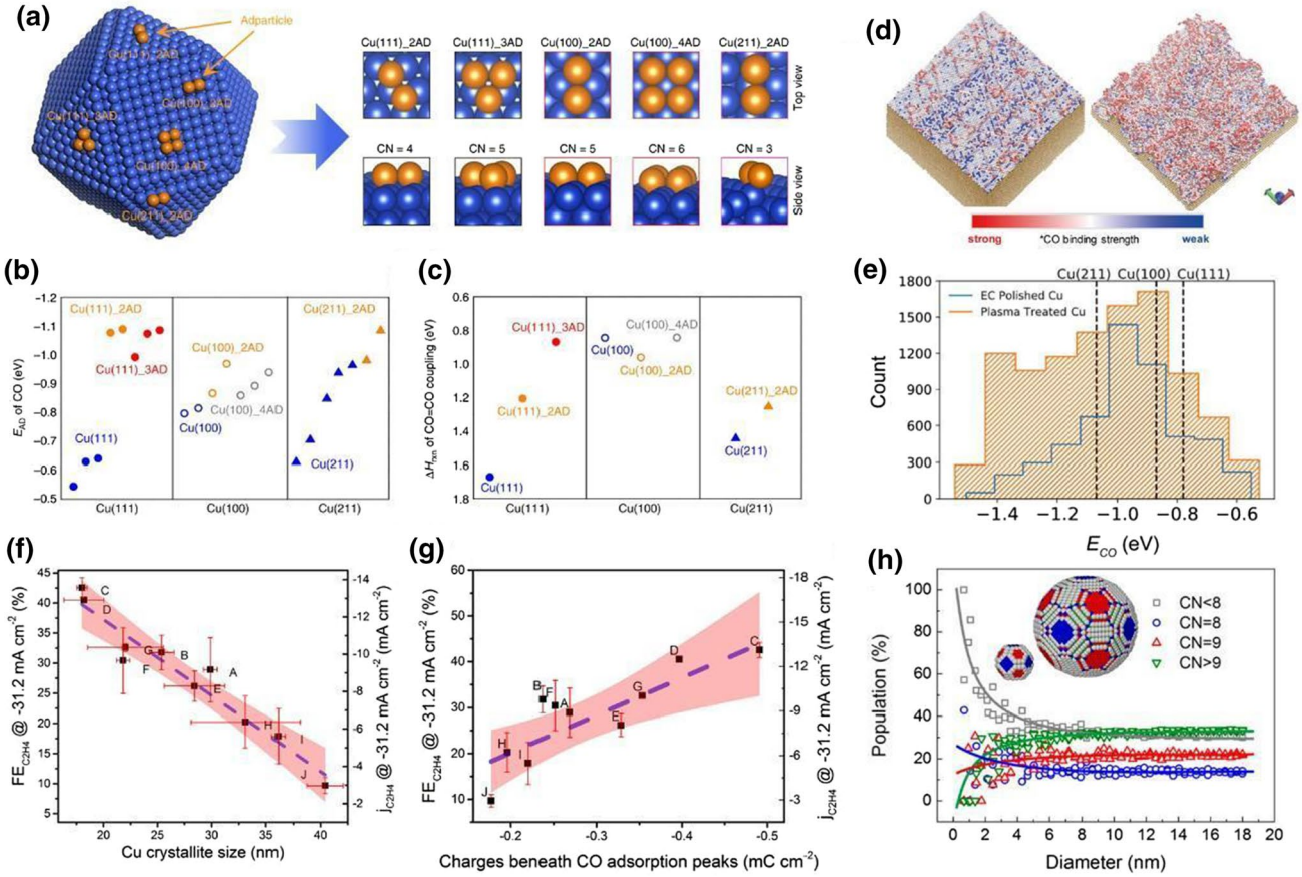

Fig. 4 Improvement of C_{2+} selectivity by unsaturated coordination atoms. **a** Demonstration of various low coordination number (CN) Cu sites with different numbers of Cu adatoms (ADs) added on various Cu facets. **b** The adsorption energy of CO. **c** The reaction energies of *CO dimerization. Reproduced with permission from Ref. [83]. Copyright 2018 Springer Nature. **d** Images of the computationally produced electropolished Cu surface (left) and the surface after Ar plasma bombardment (right). **e** Predicted distribution of CO adsorption energies. Reproduced with permission from Ref. [86]. Copyright 2020 American Chemical Society. **f** A correlation plot between the FE of C_2H_4 (FE_{C2H4}) and partial current density of C_2H_4 (j_{C2H4}) values with the crystallite sizes. **g** A correlation plot between the charges of the CO adsorption peaks with FE_{C2H4} and j_{C2H4}. Reproduced with permission from Ref. [88]. Copyright 2016 American Chemical Society. **h** Population of surface atoms with a specific CN as a function of particle diameter. Reproduced with permission from Ref. [89]. Copyright 2014 American Chemical Society

the results show that a high percentage of undercoordinated Cu sites preferentially bind to *CO (Fig. 4d, e) [86]. These results illustrate that the undercoordinated sites formed by the nanostructuring of catalysts greatly increase the activity and selectivity of C_{2+} products.

In addition, the size of nanocatalysts also influences the concentration of unsaturated atoms. Consider the example of a Cu nanocrystal cube, for which the percentage of low coordination atoms on corners and edges decreases with the increasing size of the cube; therefore, the surface structure of the nanocrystal cube is closer to that of a single crystal [87]. Cu_2O-derived Cu particles were selected to investigate the correlation between the statistical microcrystal size and selectivity of CO_2 electroreduction to C_2H_4 [88]. With a decrease in the microcrystal size from 41 to 18 nm, the selectivity of C_2H_4 increased linearly from 10 to 43% (Fig. 4f). The cyclic voltammetric analysis of Cu particles was performed in CO- and N_2-saturated electrolytes, and the results revealed a linear correlation between the adsorption charge and the selectivity of C_2H_4. This implies that smaller particles have more sites available for CO adsorption (Fig. 4g). However, hydrocarbon selectivity is sharply inhibited when the nanoparticles are smaller than 5 nm [89]. This is because the stronger binding of *CO and *H on atoms with CN < 8 largely reduces the surface mobility of intermediates, which results in a lower probability of subsequent CO hydrogenation to form hydrocarbons (Fig. 4h). Rong et al. [90] synthesized Cu catalysts with a size gradient from single atoms to nanoclusters on a graphdiyne substrate by an alkyne-bond-directed site-trapping method. Surprisingly, the increased size remarkably improved the selectivity of CORR, showing a high C_{2+} FE of 91.2% at 312 mA/cm^2 for 1–1.5 nm Cu nanoclusters with a large number of low CN atoms. These results indicate that Cu nanoparticles of size between 5 and 18 nm with moderately unsaturated coordination can exhibit suitable *CO and *H binding energies for C_{2+} production. Thus, this result highlights the practicality of unsaturated coordination atoms.

Grain Boundaries

Li et al. [91] first discovered that the reduction of Cu oxides greatly increases the catalytic performance compared to the performance of pure Cu. This increase is attributed to the abundant grain boundary (GB) structure on the oxide-derived Cu (OD-Cu). Electroreduction and H_2 annealing reduction were performed to reduce Cu_2O to Cu, and similar networks of interconnected nanocrystals with distinct GBs between the nanocrystals were obtained [92]. To investigate the effect of numerous GB structures in OD-Cu on CO_2RR and CORR performances, a series of intensive mechanistic explorations and discussions were performed by Kanan's group [34–36, 93]. The CO temperature-programmed desorption results reveal that the binding of CO on OD-Cu is stronger than that on a Cu foil, hence improving the catalytic performance of CORR for OD-Cu (Fig. 5a, b) [35]. The direct correlation between CORR activity and GB density was further quantified to establish a design principle for solid catalysts [93]. The bulk electrolysis of Cu nanoparticles with different GB densities reveals that the specific activity of CO reduction depends linearly on the ratio of GB surface terminations (Fig. 5c). Finally, GB terminations on the electrode surface are more active for CO_2RR than for HER; this finding was confirmed by scanning electrochemical cell microscopy and electron backscatter diffraction studies (Fig. 5d, e) [36]. The surface-terminating dislocations accumulated at the GBs modify the density of undercoordination sites, selectively increasing the activity of CO_2RR [34]. In addition, some research groups reported that GB structures have an excellent electrocatalytic performance for CO_2 reduction to C_{2+} products [94–100]. This performance is attributed to the facilitated CO_2 activation [94, 95], increased *CO adsorption energy [96, 97], and reduced C–C coupling barriers [98, 99].

Because *CO with a low vibrational frequency has been observed on the surface, fragmented Cu is considered to be active for rapid CO dimerization (Fig. 5f) [101, 102]. Moreover, the highly fragmented Cu also assists in clustering the binding sites of the C_1 and C_2 intermediates, thereby facilitating further coupling of these intermediates (Fig. 5g) [94, 103]. Adjusting the atomic-level spacing (atomic-d_S) between Cu particles is another efficient approach to achieve the highly active and selective generation of C_{2+} products [48]. Metallic Cu-based catalysts with different particle spacings were constructed by lithiation, delithiation, and electroreduction of CuO_x particles. The spacing range was confirmed by examining three-dimensional tomographs obtained using a Cs-corrected scanning transmission electron microscope. Theoretical and experimental results show that a spacing of 5–6 Å maximizes the binding energy of the intermediates involved in C–C bond formation, achieving a FE of ~ 80% for C_{2+} products (Fig. 5h). These results further confirm the essential effect of GBs on C_{2+} activity and selectivity.

Vacancies

Vacancy engineering enables the alteration of the surface electron structure of catalysts, thereby facilitating CO_2 activation and intermediate adsorption to generate C_{2+} products. For example, Cu surface vacancies with a Cu_2S core increase the energy barrier of the ethylene pathway but leave the ethanol pathway virtually uninfluenced; thus, a selective conversion of CO_2 to polyalcohol is achieved (Fig. 6a–e) [104]. To accurately regulate the percentage of vacancies on Cu-based catalysts, the lithium electrochemical tuning

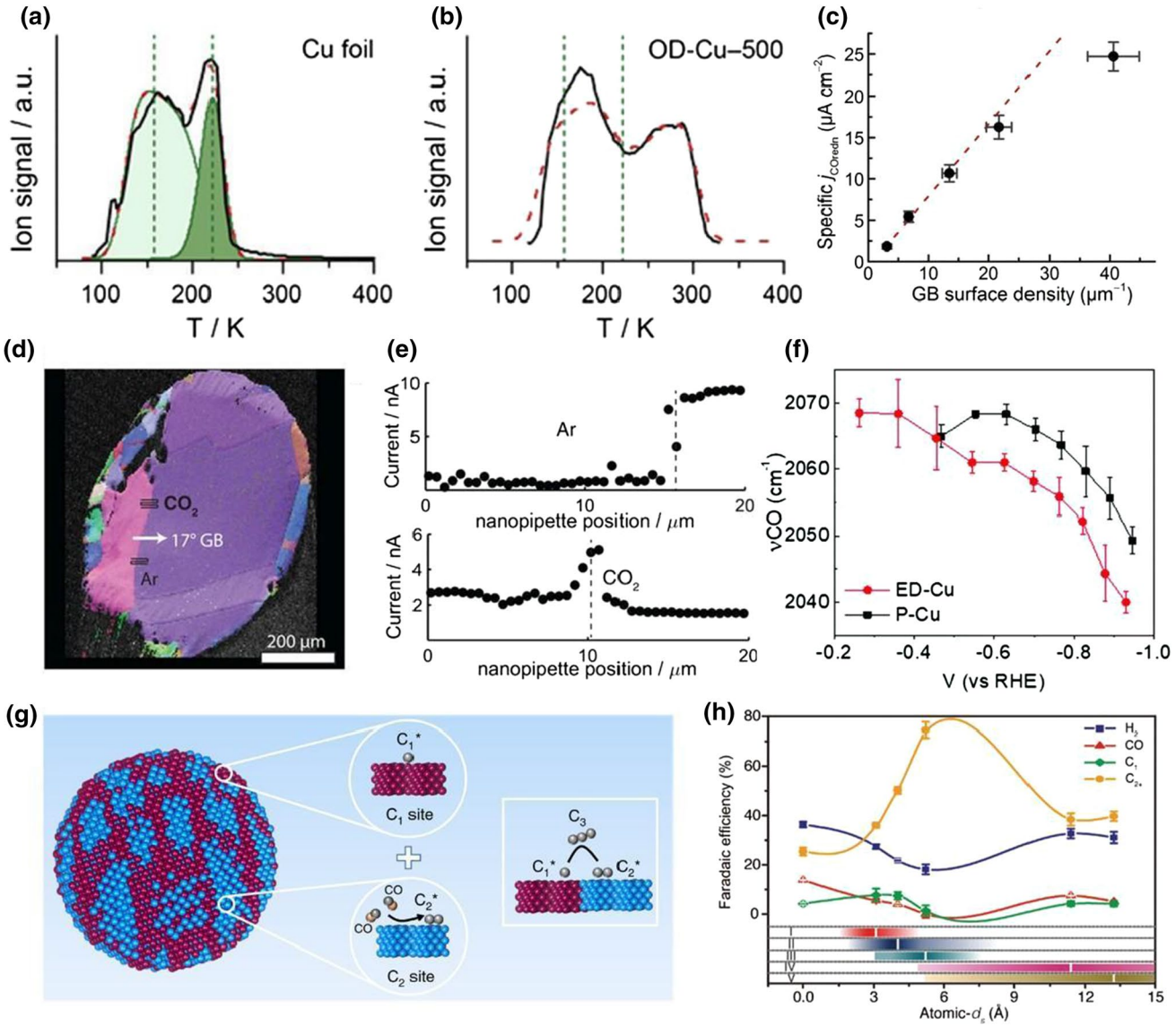

Fig. 5 Improvement of C_{2+} selectivity by grain boundaries. **a, b** CO temperature-programmed desorption profiles of **a** polycrystalline Cu and **b** oxide-derived Cu (OD-Cu) under air oxidation at 500 °C (i.e., OD-Cu–500). Reproduced with permission from Ref. [35]. Copyright 2015 American Chemical Society. **c** Specific activity for CO reduction versus the grain boundary (GB) surface density at − 0.5 V vs. a reversible hydrogen electrode (RHE). Reproduced with permission from Ref. [93]. Copyright 2016 American Chemical Society. **d** Electron backscatter diffraction orientation map of the tested sample with GBs. Inset text and paths indicate the locations where line scans were collected. **e** Line scan generated from individual constant potential electrolysis across the GB at 1 atm Ar or CO_2. Reproduced with permission from Ref. [36]. Copyright 2017 the American Association for the Advancement of Science. **f** CO vibrational frequency (νCO) observed during chronoamperometric scans. Reproduced with permission from Ref. [102]. Copyright 2020 the Royal Society of Chemistry. **g** Physical proximity of the optimal C_1 and C_2 sites that facilitate the coupling of C_1–C_2 into C_3 products. Reproduced with permission from Ref. [103]. Copyright 2019 Springer Nature. **h** The FE versus the size of the atomic-scale interspace (atomic-d_S) measured at − 0.9 V versus RHE. Reproduced with permission from Ref. [48]. Copyright 2020 Wiley–VCH

method was proposed to remove anions while preserving the nanostructure of the electrode. In this method, double S vacancies are formed on the hexagonal CuS (100) surface, and the density of the S vacancies can be regulated by controlling the number of charging–discharging cycles (Fig. 6f) [21]. The unique double S vacancy structure provides efficient electrocatalytic active sites to stabilize *CO and *OCCO dimers simultaneously, and these sites facilitate the CO–OCCO coupling to form C_3 species with an FE of 15.4% toward *n*-propanol in H-cells (Fig. 6g). In conclusion, the local electron-rich environment at the vacancy sites favors electron transfer to the CO_2RR intermediates, thereby

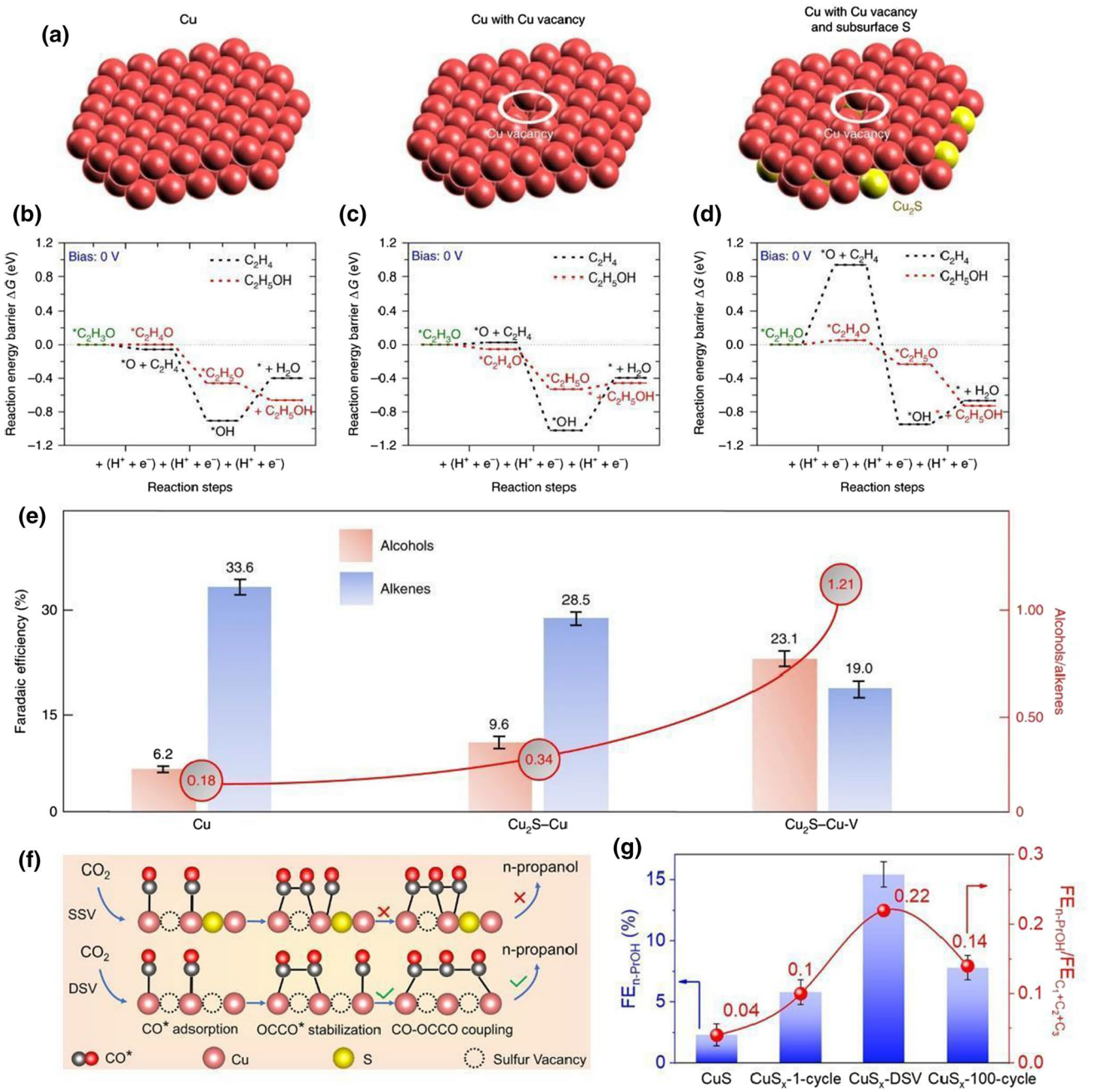

Fig. 6 Modulation of intermediate adsorption by vacancy. **a–d**: **a** Atomic models and **b** the reaction Gibbs free energy diagram from the adsorbed $*C_2H_3O$ intermediate to ethylene and ethanol for pristine Cu, **c** Cu with Cu vacancy and **d** Cu with Cu vacancy and subsurface S slab models. **e** The FE of alcohols and alkenes on various catalysts, where V denotes vacancy. Reproduced with permission from Ref. [104]. Copyright 2018 Springer Nature. **f** Mechanism of *n*-propanol formation on adjacent CuS_x with a double-sulfur vacancy (CuS_x-DSV). **g** $FE_{n\text{-PrOH}}$ and $FE_{n\text{-PrOH}}/FE_{C1+C2+C3}$ of various catalysts. Reproduced with permission from Ref. [21]. Copyright 2021 Springer Nature

facilitating the coupling of the intermediates to generate C_{2+} products. However, the stability of the S vacancies at cathodic potentials needs to be determined in future studies by in situ characterization.

Additional Element Introduction

Heteroatom Doping

Heteroatom doping has been demonstrated as an efficient way to increase active site exposure. Because of the lattice

mismatch between the dopant and Cu, the strain generated at the interface adjusts the electronic structure and the intermediate adsorption strength for CO_2RR. Doping by *p*-block elements with higher electronegativity than Cu will induce the presence of oxidation states without a phase change [105–107]. In addition, the dopants with strong oxygen affinity facilitate the breaking of C–O bonds in *$OCHCH_2$; this condition thermodynamically favors the generation of ethylene and ethane but inhibits the formation of ethanol [108]. Zhou et al. [37] found that B doping can tune the local electronic structure of Cu via the transfer of electrons from Cu to B; thus, B doping can regulate the active site ratios ($Cu^{\delta+}$ to Cu^0). B doping also persistently stabilizes $Cu^{\delta+}$ to facilitate the adsorption and dimerization of CO, and thus, there is a high tendency for C_2 formation (Fig. 7a–c). To further improve the long-term stability of C_{2+} production, Zn atoms were introduced in the B-doped Cu [109, 110]. Recently, F-doped Cu was demonstrated to promote water activation, and the resulting local enrichment of *H facilitates the hydrogenation of *CO to *CHO, which in turn lowers the C–C coupling energy barrier and promotes the formation of C_{2+} products [111]. Similarly, Cu-based catalysts derived from metal–organic framework (MOF) with different organic linkers were used to reveal the mechanism for C_{2+} generation [112]. The C_2/C_1 product ratios can be adjusted from 0.6 to 3.8 following the order $NH^{2-} < OH^- <$ bare $< F^- < 2F^-$, suggesting that the

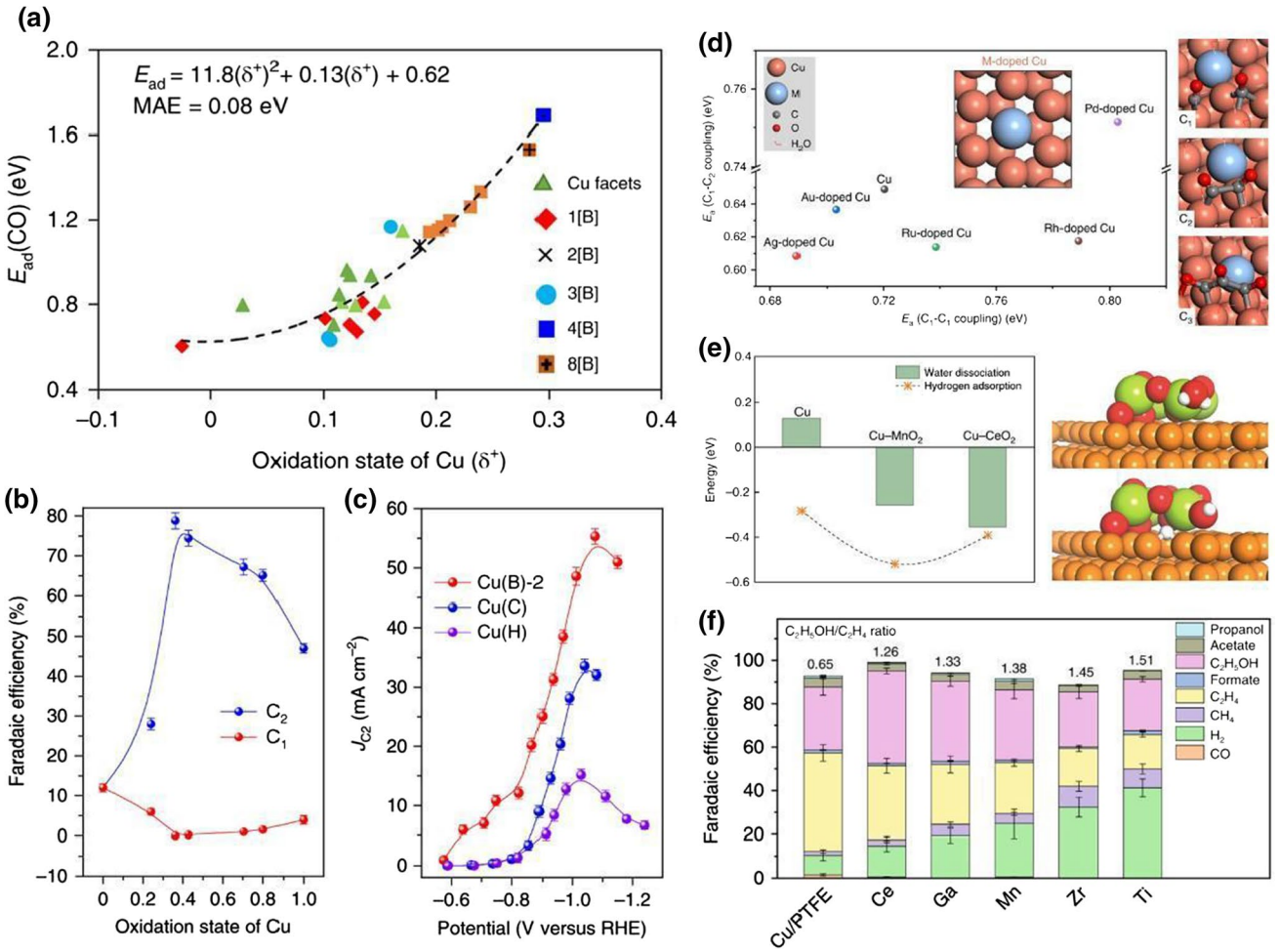

Fig. 7 Modulation of intermediate adsorption by doping. **a** CO adsorption energy as a function of the oxidation state of Cu. **b** The FE of C_2 and C_1 for different oxidation states of Cu on B-doped Cu (Cu(B)). **c** The partial current density of C_2 at different potentials on Cu(B)-2, oxidized nano-Cu (Cu(C)), and pristine Cu (Cu(H)). Reproduced with permission from Ref. [37]. Copyright 2018 Springer Nature. **d** Reaction barriers for C_1–C_1 and C_1–C_2 coupling on M-doped Cu systems calculated based on the density functional theory (DFT). Reproduced with permission from Ref. [59]. Copyright 2019 Springer Nature. **e** Calculated water dissociation reaction energies and hydrogen adsorption energies on various surfaces. **f** Product distributions of various hydroxides/oxide-modified Cu/PTFE electrodes, along with the corresponding C_2H_5OH/C_2H_4 ratio. Reproduced with permission from Ref. [19]. Copyright 2019 Springer Nature

increased dissociation of H_2O by strongly electronegative groups in organic linkers favors C_2 production.

Since the electrosynthesis of C_3 products depends greatly on the presence of both C_1 and C_2 intermediates, metal doping strategies were proposed to achieve the simultaneous stabilization of these intermediates. Among metal-doped Cu candidates, Ag-doped Cu favors both C_1−C_1 coupling and C_1−C_2 coupling. This Ag-doped Cu has the highest FE (33%) for the reduction of CO to *n*-propanol [59]. The facilitation of multiple C−C coupling is attributed to the strain and ligand effects induced by Ag doping, which result in an energetic asymmetry of the adjacent Cu atoms (Fig. 7d). Compressive strain induced by doping with Ag atoms in the Cu lattice also shifts the valence band density of Cu to a deeper level [113]. This electronic structure lowers the binding energies of H and O compared to the binding energy of CO, and thus, the HER is selectively inhibited, and the generation of carbonyl-containing C_{2+} products, accompanied by decreased generation of hydrocarbons, is facilitated.

Given the important role of hydrogenation reactions in multicarbon alcohol production [114, 115], heteroatom doping is also proposed to modulate the *H on the surface of catalysts for facilitating the hydrogenation of intermediates after C−C coupling. Theoretical calculations revealed that Pt- or Pd-doped Cu exhibits the optimal H binding energy, which promotes the hydrogenation of C_2 intermediates to generate C_2H_5OH [116]. The results show that the CuPd and CuPt catalysts have an alcohol-to-ethylene FE ratio that is twice that of bare Cu. In addition, hydroxide- and oxide-doped Cu catalysts stabilized at reduction potential can also activate water and tune the surface *H coverage, thereby regulating the ethanol and ethylene reaction pathways (Fig. 7e) [19]. The increased *H is only involved in the branched reaction toward ethanol, accelerating the conversion of *HCCOH to *HCCHOH (a key intermediate for ethanol generation). Among all the hydroxide- and oxide-doped Cu catalysts, $Ce(OH)_x$/Cu/PTFE exhibits the maximum FE of 43% for ethanol generation at a current operating density of 300 mA/cm^2 (Fig. 7f). In conclusion, doping affects the adsorption of different intermediates, and thus, it is thus beneficial to break the linear adsorption relationship of intermediates for the selective generation of certain C_{2+} products.

Cu-Based Alloys

Alloying is another effective strategy to modulate the electronic and geometrical structures of catalysts for inhibiting HER competition and promoting CO_2RR activity [117]. The electronic structure of the catalyst is directly correlated with the binding strength of intermediates, and the geometrical structure affects the local distribution of certain intermediates at active sites. Several Cu-based alloys were extensively studied from the viewpoint of C_{2+} production [118, 119]. For example, He's group [120] used E-beam evaporation to fabricate thin films of CuAg to precisely regulate the stoichiometric ratio of the two elements. Thus, they built a good model to reveal the real reaction mechanisms during the CO_2RR process. The *operando* synchrotron radiation–Fourier transform infrared spectroscopy (SR-FTIR) demonstrated that the CuAg bimetal greatly inhibits the formation of O−C−O intermediates and increases the coverage of *CO and *OCCO intermediates, thus promoting the C_{2+} production (Fig. 8a). Moreover, Cu supported on amorphous CuTi alloys (a-CuTi@Cu) can electroreduce CO_2 to C_{2-4} products, such as ethanol, propanol, and *n*-butanol (Fig. 8b) [121]. Theoretical simulations and in situ characterization demonstrate that the subsurface Ti atoms increase the electron density of the surficial Cu sites with improved adsorption ability of *CO intermediates. Thus, the energy barriers for the dimerization or trimerization of *CO are reduced. The function of the interface in Cu alloys in promoting C−C coupling and C_{2+} formation was also confirmed by theoretical calculations [122].

To expedite the discovery of Cu-based catalysts with high C_{2+} selectivity, Sargent's group [123] developed a machine learning-accelerated high-throughput DFT framework for material selection. They selected 228,969 adsorption sites from 244 different Cu-containing intermetallic compound crystals to train a machine learning model. The framework was subjected to approximately 4000 DFT simulations for CO adsorption energy calculations, and the Cu-Al alloy exhibited the highest abundance of adsorption sites and site types with near-optimal CO adsorption energies. These properties created a favorable Cu coordination environment for C–C dimerization (Fig. 8c, d). The rationally designed Cu-Al electrocatalysts show a high C_2H_4 FE of 80% at a current density of 400 mA/cm^2. Thus, Sargent's group [123] demonstrated the essential role of high-throughput screening based on the adsorption energy of key intermediates in the development of Cu-based bimetallic catalysts, and they accelerated the targeted design of catalysts with high C_{2+} selectivity. Weitzner et al. [119] calculated the *CO dimerization energies on different Cu-based alloys, and they found that Cu-Al alloys favor the dimerization reaction of *CO. In general, alloying is a promising approach to tuning the adsorption energy of intermediates by manipulating the electronic structure of Cu catalysts. Thus, alloying is extremely helpful in facilitating the efficient generation of C_{2+} products.

Chemical State Effects

The adjustment of the valence state of Cu can modify the electronic structure of Cu-based catalysts, thus improving the catalytic performance. Some studies suggest the presence of oxidized Cu plays a crucial role in converting CO_2

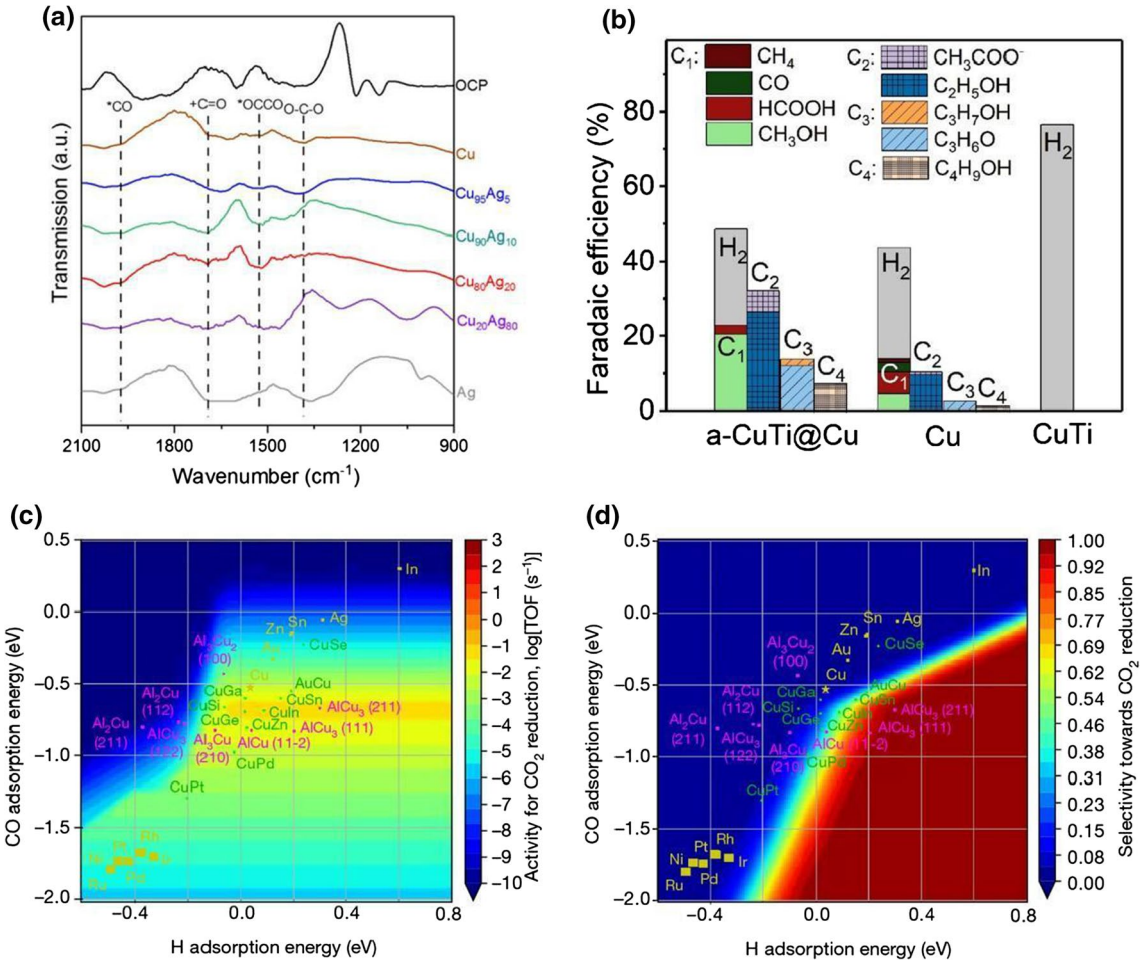

Fig. 8 Modulation of intermediate adsorption by Cu-based alloys. **a** *Operando* synchrotron radiation–Fourier transform infrared (SR-FTIR) spectroscopy during CO_2RR. Reproduced with permission from Ref. [120]. Copyright 2022 American Chemical Society. **b** FE for various electrocatalysts at − 0.8 V versus RHE. Reproduced with permission from Ref. [121]. Copyright 2021 Wiley–VCH. **c** A two-dimensional activity volcano plot for CO_2RR. **d** A two-dimensional selectivity volcano plot for CO_2RR. Reproduced with permission from Ref. [123]. Copyright 2020 Springer Nature

to C_{2+} products via ex situ characterizations [95, 124]. However, Cu is highly susceptible to reoxidation at the open circuit potential [71], and the real valence state of Cu under operating conditions remains controversial, limiting the mechanistic understanding of Cu-based catalysts. To clarify whether the oxidized Cu exists at an extremely negative potential during the CO_2RR, isotopic labeling was used in the preparation process of Cu oxides, and only < 1% ^{18}O remanence in the ^{18}OD-Cu was discovered after a 5 h CO_2RR electrolysis (Fig. 9a) [125]. Lei et al. [126] investigated the distribution of various Cu species on electrodes by high-angle annular dark-field scanning transmission electron microscopy (HAADF-STEM) and electron energy loss spectroscopy (EELS) and found that oxidized Cu was completely reduced to metallic Cu during CO_2RR, regardless of the initial state (Fig. 9b). Further, based on DFT modeling, Mandal et al. [127] suggested that the reduction of Cu_2O is kinetically and energetically more favorable than that of CO_2RR, implying that oxidized Cu should be reduced to metallic Cu before forming CO_2RR products.

Conversely, using in situ characterization techniques, some researchers found that Cu^+ and residual subsurface oxygen can exist even at negative potentials [128, 129]. Cuenya and coworkers [129] provided experimental evidence for the survival of Cu^+ species during CO_2RR via *operando* X-ray absorption spectroscopy (Fig. 9c). They revealed that Cu^+ significantly inhibits CH_4 production and thus increases the FE of C_2H_4 (Fig. 9d). Yang et al. [130] synthesized Cu nanocavity catalysts to confine carbonaceous intermediates, which in turn cover the catalyst surface to protect the Cu^+ species, and they achieved a C_{2+} FE of 75.2%. In addition, the coexistence of Cu^0 and Cu^+ on the surface affects the CO_2RR selectivity by changing the CO adsorption configuration. The top-adsorbed CO (CO_{atop})

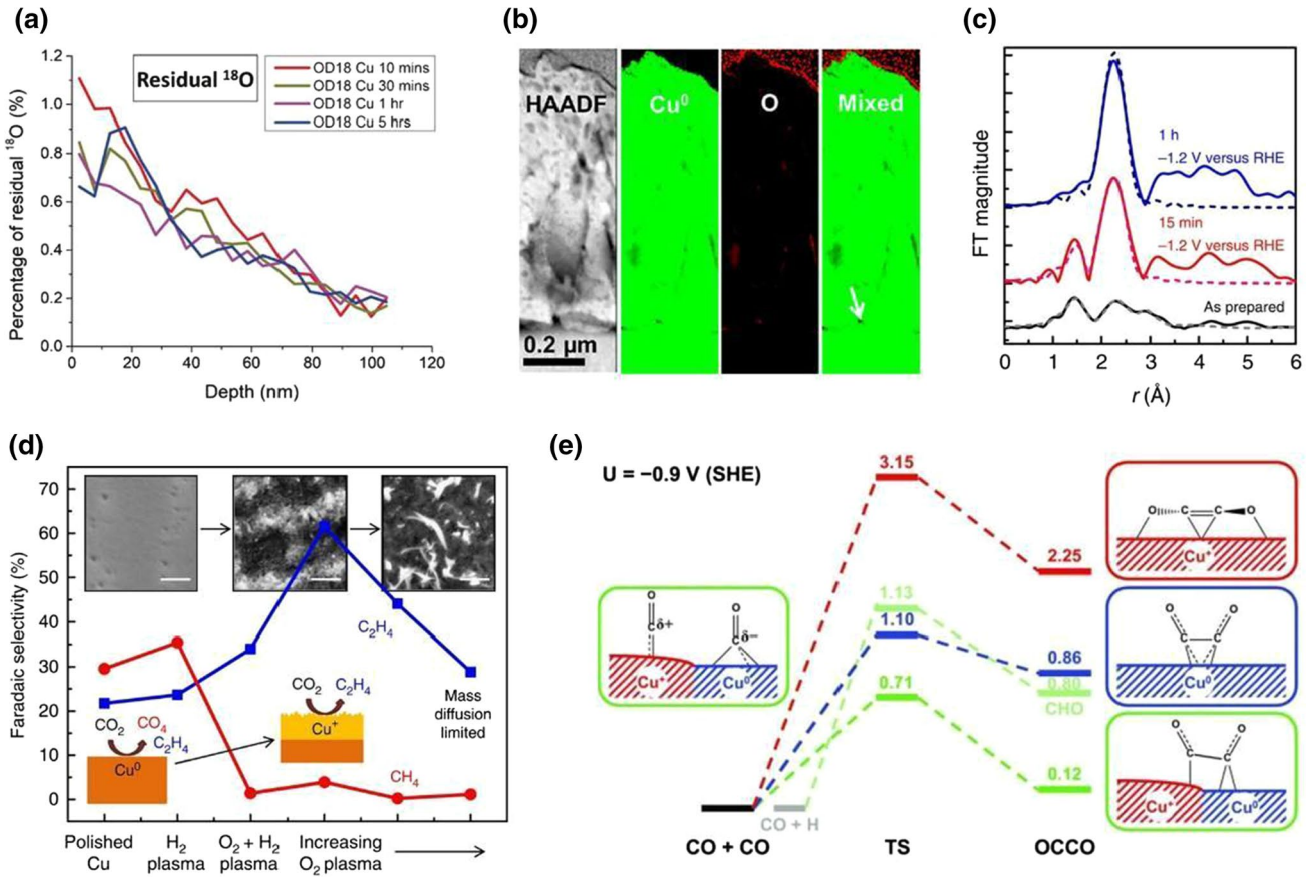

Fig. 9 Improvement of C_{2+} selectivity by chemical state effects. **a** ^{18}O percentage of OD-Cu catalysts at different CO_2 reduction catalytic times. Reproduced with permission from Ref. [125]. Copyright 2018 Wiley–VCH. **b** High-angle annular dark-field scanning transmission electron microscopy (HAADF-STEM) images and electron energy loss spectroscopy (EELS) mapping of the cross section of HQ-Cu after 1 h of CO_2RR. Reproduced with permission from Ref. [126]. Copyright 2020 American Chemical Society. **c** Extended X-ray absorption fine structure spectra of different catalysts under *operando* conditions. **d** Summary of the activity of plasma-treated Cu electrodes. Reproduced with permission from Ref. [129]. Copyright 2016 Springer Nature. **e** The DFT calculation of CO dimerization and CO hydrogenation toward CHO over mixed Cu^0/Cu^+ catalyst. Reproduced with permission from Ref. [132]. Copyright 2017 National Academy of Sciences

intermediates are mainly observed on Cu^+ sites, while the bridge-adsorbed CO (CO_{bridge}) intermediates are mainly observed on Cu^0 sites [131]. The adjacent-adsorbed CO_{bridge} and CO_{atop} are negatively and positively charged, respectively, because of which they are beneficial for CO dimerization (Fig. 9e) [132]. Despite these promising results, the catalytic role of oxidized Cu still remains a debated issue, and further advances in *operando* techniques are required to resolve this issue.

Electric Field Effects

The stabilizing effect of electric fields on intermediates (e.g., *CO or *COCO), as demonstrated by theoretical calculations, makes it a promising method to manipulate the reaction pathways by regulating the applied electric field [47]. Sargent's group [133] investigated the effect of an intensified electric field on localized CO_2 enrichment. They used a metallic nanotip electrode to generate a locally high electric field at low overpotentials. In their work, the cations were concentrated around the sharp tip, leading to an increased local concentration of CO_2 near the active surface for CO_2RR. The electric field-induced effect on the concentration of reagents around the tips was also analyzed using kinetic simulations, indicating that the electric field-induced aggregation effect can provide additional CO_2 for improving the CO_2RR performance [134, 135]. Recently, Liu's group [136, 137] also reported that the high electric field created locally by high-curvature Cu nanoneedle (Cu NN) arrays can optimize *CO adsorption and reduce C−C coupling energy barriers (Fig. 10a). Besides, encapsulating the Cu NNs in polytetrafluoroethylene (PTFE) conformal coatings was proposed as a typical strategy to enhance the local electric and thermal fields simultaneously (Fig. 10b) [138, 139].

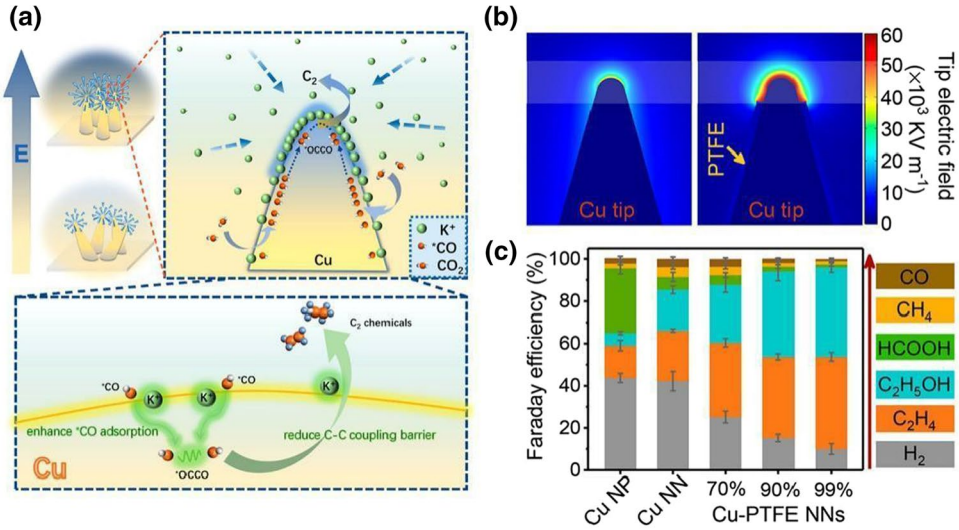

Fig. 10 Improvement of C_{2+} selectivity by electric field effects. **a** Schematic diagram of C_2 formation process on the single tip of Cu nanoneedle (NN) arrays. Reproduced with permission from Ref. [137]. Copyright 2022 American Chemical Society. **b** The electric field distribution on a pristine Cu NN (left) and on a Cu NN with 99% PTFE coverage (Cu-PTFE NN) (right). **c** Product distribution and corresponding FEs. Reproduced with permission from Ref. [138]. Copyright 2022 American Chemical Society

DFT calculations indicated that the enhanced electric field reduces the Gibbs free energy of the C−C coupling, while increasing the thermal field intensity boosts the reaction rate of C−C coupling; thus, a CO_2-to-C_2 FE of over 86% can be achieved (Fig. 10c). To summarize, a locally enhanced electric field effectively enhances the adsorption strength of CO_2 and intermediates and reduces the C−C coupling energy barriers, thus enabling the highly selective production of C_{2+} at the sharp tip catalytic hotspots.

Substrate Effects

Although catalyst substrates are primarily used to load catalysts and provide electron-conductive channels, their structures also affect CO_2RR performance, resulting in the so-called "substrate effects." Specifically, the substrates can not only affect the reconstruction of Cu nanoparticles, but also have electronic interactions with active Cu sites [140]. Because of the outstanding chemical and electrochemical stability of carbon materials, they are the most widely used substrates. Since N has strong CO_2 adsorption capability, N-doped substrates can increase the local CO_2 concentration and enrich the key intermediates of C−C coupling [141]. For example, N-doped nanodiamonds (N-ND) were used as substrates for sputtered Cu nanoparticles, and an FE of 63% was realized for C_2 oxygenates at − 0.5 V vs. RHE (Fig. 11a) [142]. DFT calculations indicate that the increased *CO binding at the interface between the Cu nanoparticles and an N-doped nanodiamond substrate suppresses the *CO desorption and reduces the barriers to *CO dimerization, thus promoting C_2 production (Fig. 11b, c). The similar synergy between N-doped carbon nanospikes and loaded Cu nanoparticles was demonstrated for the highly selective conversion of CO_2 to C_2H_5OH [143].

The substrate also affects the reconstruction process of Cu during CO_2RR, thereby altering product selectivity. Cu cubes on carbon paper were observed to undergo drastic morphological and compositional changes during the CO_2RR with selective inhibition of the C_{2+} products relative to CH_4 [144]. This is caused by the physical separation of the active sites on the carbon substrates with high specific surface areas. However, as the electrolysis duration increases, the C-supported Cu nanocubes also gradually agglomerate, leading to the transition of CO_2RR products from C_1 to C_2 again (Fig. 11d) [145]. Hence, a reasonable selection of substrates and the dispersion of active sites are crucial to be able to make full use of the substrate effects.

Confinement Effects

Spatial confinement effects can change the mass transfer process and optimize the local distribution of intermediates [146]. Constructing porous Cu electrodes is a typical method of altering the mass transfer based on the specific confinement effect of pores. Increasing the pore depth results in locally higher pH and lower CO_2 concentration inside the pore, and this effect can be intensified by increasing the cathodic potential [147, 148]. Changes in the local environment caused by mass transfer further affect the product distribution of the CO_2RR. For example, C_1 products strongly depend on the local concentration of CO_2, while C_2 products tend to be formed in a locally high pH environment [63]. Besides, confinement effects can also restrict the diffusion of intermediates via the formation of closed spaces. Cu nanocavities can limit the efflux of C_2 intermediates, thereby increasing the coverage and retention time of the intermediates required for C_3 production. Finite element simulations revealed that the cavity-opening angles play critical roles in the C_3/C_2 selectivity ratio (Fig. 12a). An opening of ~ 60° is

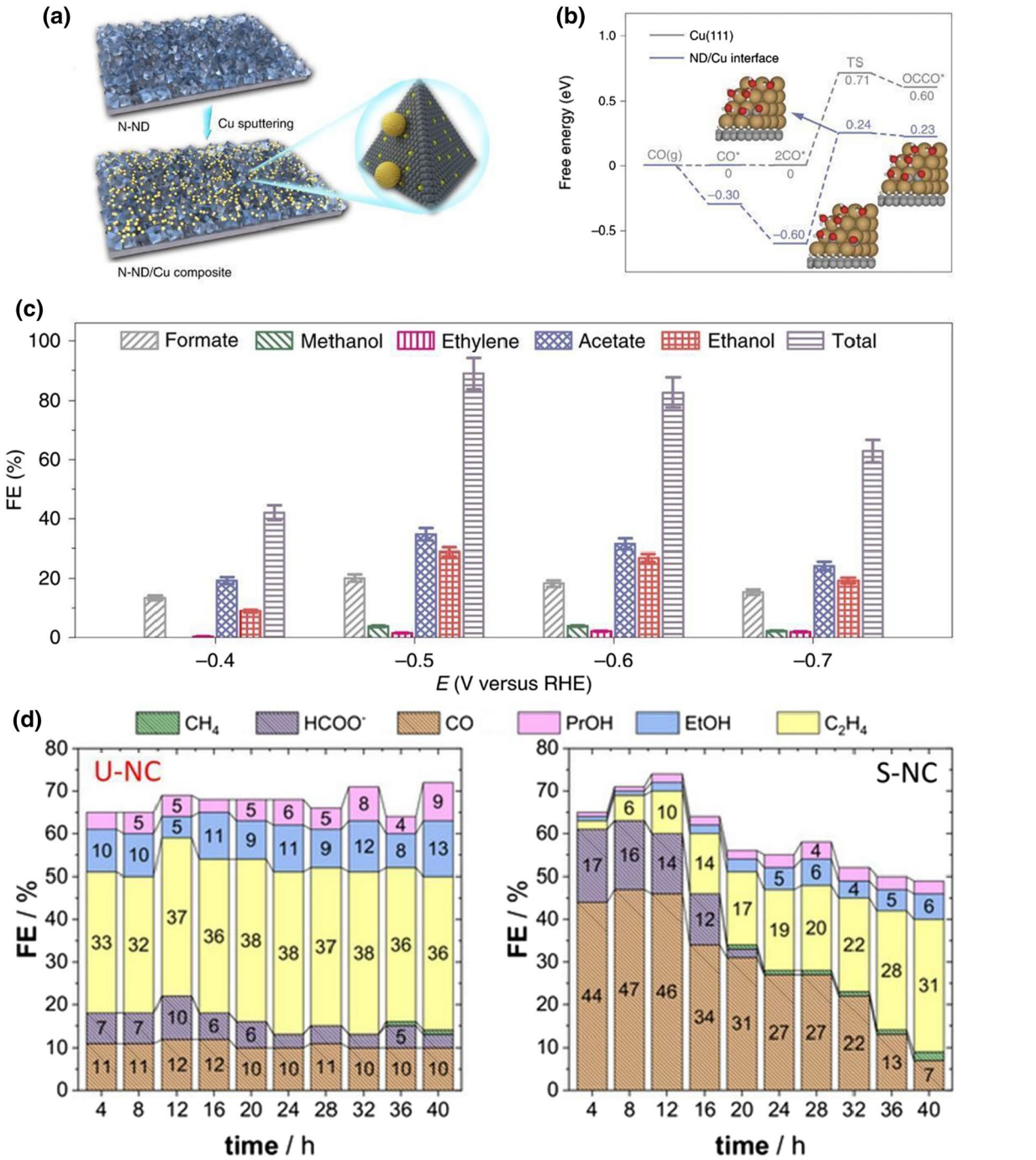

Fig. 11 Substrate effect for improving C_{2+} selectivity. **a** Schematic illustration of the preparation of N-doped nanodiamond (N-ND)/Cu composite materials. **b** Free energy diagram for CO coupling. **c** FE values for carbon-containing products by N-ND/Cu electrodes. Reproduced with permission from Ref. [142]. Copyright 2020 Springer Nature. **d** Results of 40 h stability test at − 300 mA/cm^2, where FE is shown as a function of time for unsupported Cu nanocubes (U-NC) and for C-supported nanocubes (S-NC). Reproduced with permission from Ref. [145]. Copyright 2020 Wiley–VCH

the most favorable for C_3 production, where the enrichment of C_2 intermediates is not limited by the reduced CO availability (Fig. 12b, c) [149]. Hollow porous Cu nanospheres, hollow multishelled Cu, and multishelled CuO microboxes were also reported to show similar confinement effects. The high C_{2+} selectivity is attributed to the C−C coupling facilitated by the high coverage of carbonaceous intermediates in the cavity [150–152].

Confinement effects can also be exploited to design tandem catalysts to reutilize the products of CO-selective

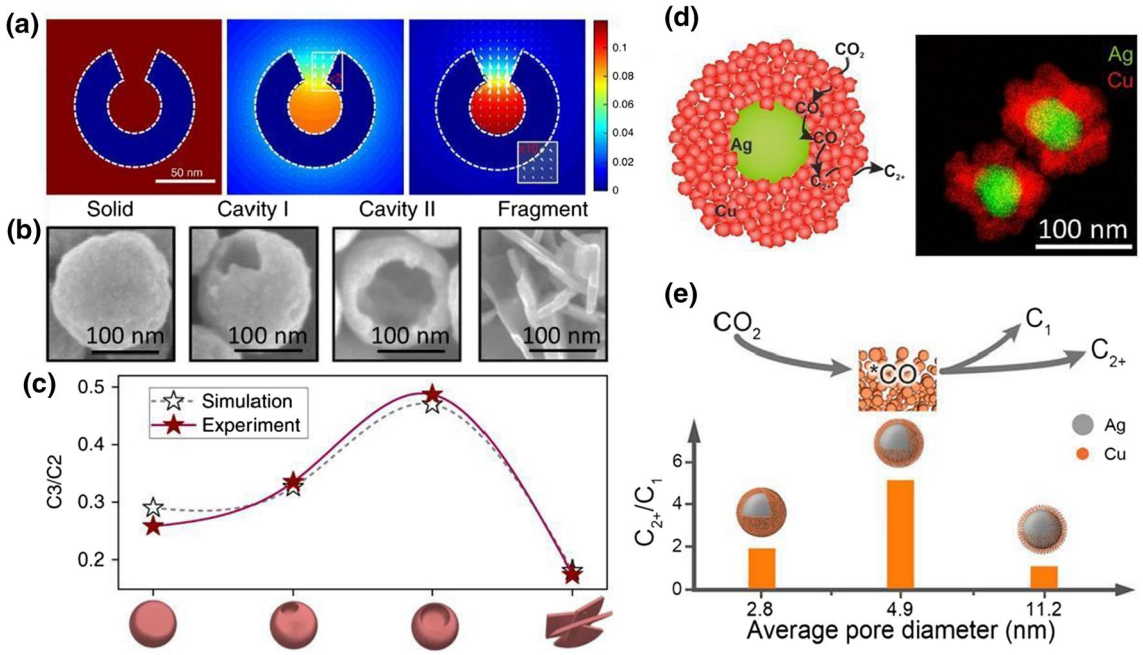

Fig. 12 Improvement of C_{2+} selectivity by confinement effect. **a** CO (left), C_2 (middle), and C_3 (right) concentrations (color scale, in millimoles) and flux distributions (arrows) on the cavity confinement structure. **b** Representative scanning electron microscopy images of different catalysts. **c** C_3/C_2 product selectivity on different catalysts obtained from experiments and from finite element simulations. Reproduced with permission from Ref. [149]. Copyright 2018 Springer Nature. **d** Schematic representation and compositional characterization of the Ag core/porous Cu shell particle. Reproduced with permission from Ref. [153]. Copyright 2021 Wiley–VCH. **e** The C_{2+}/C_1 product selectivity on the Ag@Cu catalysts with different average pore diameters at 400 mA/cm^2. Reproduced with permission from Ref. [154]. Copyright 2022 American Chemical Society

catalysts. For example, nanoparticles with Ag cores and porous Cu shells can simultaneously use the CO overflow from the Ag cores and confinement effects of the porous Cu channels (Fig. 12d) [153]. In this system, CO_2 is selectively reduced to CO on the Ag core at the bottom of the porous Cu channel, while a prolonged diffusion time provides more opportunities for the porous Cu shell to reduce the substrate-enriched CO to C_{2+} products. The C_{2+}/C_1 product selectivity can be further increased by optimizing the diameter of the channels (Fig. 12e) [154]. Therefore, the confinement effects that can alter the electrolyte environment and locally enriched intermediates are a highly effective strategy to improve the utilization of carbonaceous intermediates for C_{2+} products.

Local Microenvironment Effects

Regulation of the local microenvironment near the catalyst surface is another promising strategy to facilitate the electroreduction of CO_2 to C_{2+} products. However, many influencing factors have complex effects on the local microenvironment [155]. In this section, the effects of electrolyte composition and concentration on the local microenvironment properties, such as local pH and electrostatic interactions, are mainly discussed.

Although $KHCO_3$ solution is widely used in CO_2RR experiments to maintain neutral pH, a pH gradient exists near the electrode surface because of the OH^- formed during the reduction reaction [156, 157]. The local pH near the electrode plays an important role in the *CO/*H coverage, which determines whether *CO subsequently undergoes dimerization or hydrogenation. At lower pH values, *CO prefers to form CH_4 in the presence of abundant *H. At higher pH, where *H is scarce and *CO coverage is high, ethylene formation dominates over ethane formation [158]. As the rate of OH^- production depends on the applied potential, it is necessary to probe the local pH near the electrode under operational conditions. Lu et al. [159] designed a flow Raman electrochemical cell to measure the local pH near the gas diffusion electrode during CO_2RR (Fig. 13a). By analyzing the CO_3^{2-} and HCO_3^- concentrations in different electrolyte regions near the electrode via in situ microarea Raman spectroscopy, the corresponding pH values can be deduced from the equilibrium between HCO_3^- and CO_3^{2-}. A much higher local pH (11.9) than that of the electrolyte bulk was observed near the cathode surface (Fig. 13b). This accurate estimation of the local pH facilitated the further investigation of the pH effect during the CO_2RR. In addition, anions with buffering capacity can also alter the local pH, thus affecting the pH-sensitive reactions at the catalyst

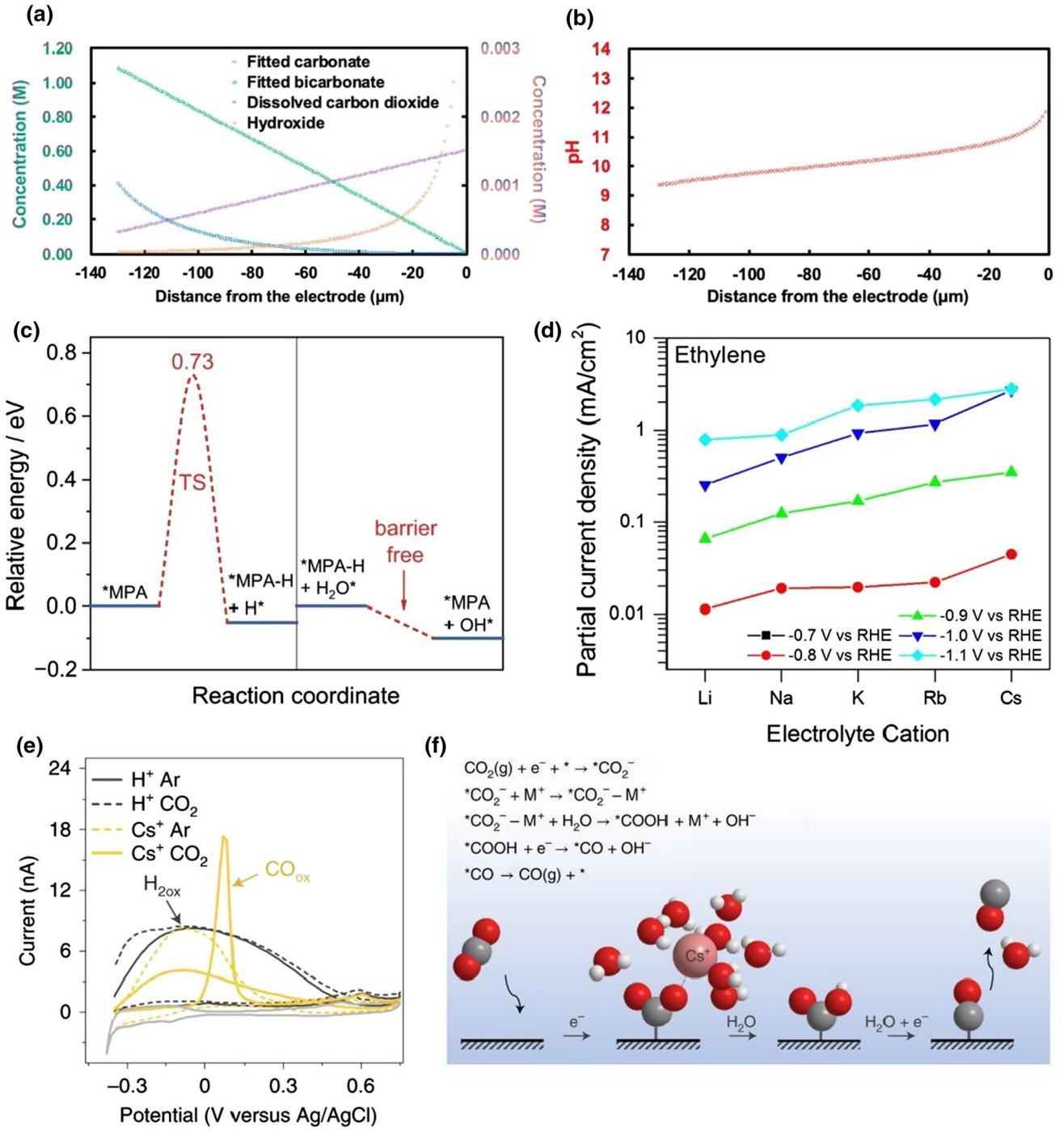

Fig. 13 Modulation of intermediate adsorption by local microenvironment. **a** Fitted concentrations of HCO_3^-, CO_3^{2-}, CO_2 (aq), and OH^- and **b** pH profile in 1 mol/L $KHCO_3$ with respect to the distance from the GDE surface. Reproduced with permission from Ref. [159]. Copyright 2020 American Chemical Society. **c** Kinetic energy diagrams of an H atom transferred from *MPA to Cu (110) and an H atom compensated from H_2O to *MPA – H. Reproduced with permission from Ref. [39]. Copyright 2022 Springer Nature. **d** Partial current densities of ethylene at different potentials as a function of the electrolyte metal cation on Cu (100). Reproduced with permission from Ref. [162]. Copyright 2017 American Chemical Society. **e** Cyclic voltammetric curves of Cu electrodes in Ar and CO_2 atmosphere after CO_2RR in 1 mmol/L H_2SO_4 with or without Cs^+. **f** Schematic representation of the interaction of the cation with the negatively charged CO_2^- intermediate. Reproduced with permission from Ref. [40]. Copyright 2021 Springer Nature

surface [160]. Buffering anions increase the selectivity of H_2 and CH_4 in the following order of decreasing pK_a: HCO_3^- (10.33) > H_3BO_3 (9.23) > HPO_4^{2-} (7.21) [161]. This finding suggests that buffer anions with pK_a lower than water can provide hydrogen directly to the electrode surface. Notably, special adsorption additives can also modulate the local proton feeding microenvironment. Our group [39] has explored boosting proton feeding toward Cu surfaces using EDTMPA additives. The adsorbed EDTMPA serves as a proton-delivering medium that accelerates the dissociation of water, providing abundant *H to assist *CO protonation toward *CHO. Typically, one H atom is transferred from the adsorbed methanephosphonic acid (*MPA, a fragment of EDTMPA) to Cu (110), and the *MPA that loses one H (*MPA − H) subsequently captures one H atom from the adjacent H_2O molecule to become an *MPA again (Fig. 13c).

In addition to local pH, the electrostatic interactions between cations and negatively charged CO_2 intermediates in the local microenvironment also have a considerable impact on CO_2RR. Bell's group [162] measured the CO_2RR performance of Cu catalysts in bicarbonate electrolytes with different alkali metal cations. The activity of ethylene formation on Cu follows the trend of atomic radius increasing in order: $Li^+ < Na^+ < K^+ < Rb^+ < Cs^+$ (Fig. 13d). Theoretical calculations suggest that the presence of solvated cations in the outer Helmholtz plane stabilizes the negatively charged reaction intermediates such as $*CO_2^-$ and $*OCCO^-$. The difference in activity when using various cations is attributed to the broader coverage of cations as the cation size increases. Recently, Koper's group [40] found that CO_2RR can only proceed on Cu when metal cations are present in the electrolyte (Fig. 13e). DFT simulations confirmed that the partially desolated metal cations stabilized the CO_2^- intermediates by short-range electrostatic interactions, thus allowing its reduction (Fig. 13f). These works highlight the necessity of cations and water in the electrochemical activation of CO_2.

In situ Characterization Techniques

To deeply understand the CO_2RR mechanisms, various in situ characterization techniques were developed to capture real-time information under actual operating conditions. To date, in situ infrared (IR) spectroscopy, in situ Raman spectroscopy, in situ mass spectrometry (MS), and in situ isotope tracer technology have been widely used to characterize the reaction intermediates to propose possible reaction pathways.

In situ IR spectroscopy was extensively used to reveal the CO_2RR mechanisms by detecting the chemisorbed species on the electrode surface [163]. Then, the adsorbed species with unique vibrational modes such as *CO, adsorbed CO_3^{2-}, and *CO dimers can be analyzed in real time during the CO_2RR. Hori and coworkers [164] first identified *CO at a Cu electrode during CO_2RR by performing in situ IR spectroscopy. Heyes et al. [56] detected the vibration bands of *CO and *H on Cu at 2060 and 2090 cm^{-1}, respectively, by performing surface-enhanced infrared absorption spectroscopy (SEIRA). Further, peak deconvolution revealed that *H can partially replace *CO, while *CO cannot replace *H (Fig. 14a). Moradzaman et al. [165] assigned the band at ~ 1610 cm^{-1} to the CO_2-dimer radical anion, which subsequently decomposed into CO_3^{2-} and *CO. The adsorbed carbonate was distinguished from the dissolved carbonate because of its strongly potential-dependent peak position in the range of 1510–1570 cm^{-1}. Koper's group [166] found that the vibrational bands at 1191 and 1584 cm^{-1} corresponding to the C–O–H and C=O stretching modes of the hydrogenated dimer (*COCOH), respectively, suggesting that the stable adsorption of *COCOH is responsible for the high C_2H_4 selectivity on Cu (100).

In situ Raman spectroscopy can effectively complement IR spectroscopy because of its relatively low response to water, which is usually used to detect varying rotational or vibrational states of different molecules on the catalyst surface [167]. The high-speed data acquisition in the case of Raman spectroscopy helps distinguish the real-time reaction intermediates. *CO is the most common CO_2RR reaction intermediate observed by in situ Raman spectroscopy, and a low-intensity carbonate signal can also be detected [168, 169]. Zhan et al. [170] found that the ratio of the intensity of the Cu–CO stretching band to that of the CO rotational band follows a volcano-shaped trend, which depends on the potential-dependent surface coverage of CO. At high CO surface coverage, the mixed adsorption conformation of CO at the top and bridge sites kinetically and thermodynamically favors C–C coupling, thereby effectively improving the C_{2+} selectivity. An et al. [101] used subsecond in situ time-resolved surface-enhanced Raman spectroscopy to reveal the dynamics of CO intermediates during the CO_2RR on Cu. A highly dynamic *CO with characteristic vibration below 2060 cm^{-1} is associated with C–C coupling and C_2H_4 production, while the isolated and stationary *CO with a distinct vibration at 2092 cm^{-1} favors the generation of gaseous CO (Fig. 14b).

Quantitative isotope measurements are indispensable for understanding the CO_2RR mechanisms at the molecular and atomic levels. Because of the different kinetic radii of different isotopes, the kinetic isotope effect (KIE) is commonly used to investigate the effect of isotopic substitution on the reaction rate to verify the potential RDS. In addition, the isotopic labeling method is usually used to reveal the origin of the intermediates or final products or both by detecting the location of the isotopically labeled atoms, thus providing suggestions of potential reaction pathways [171].

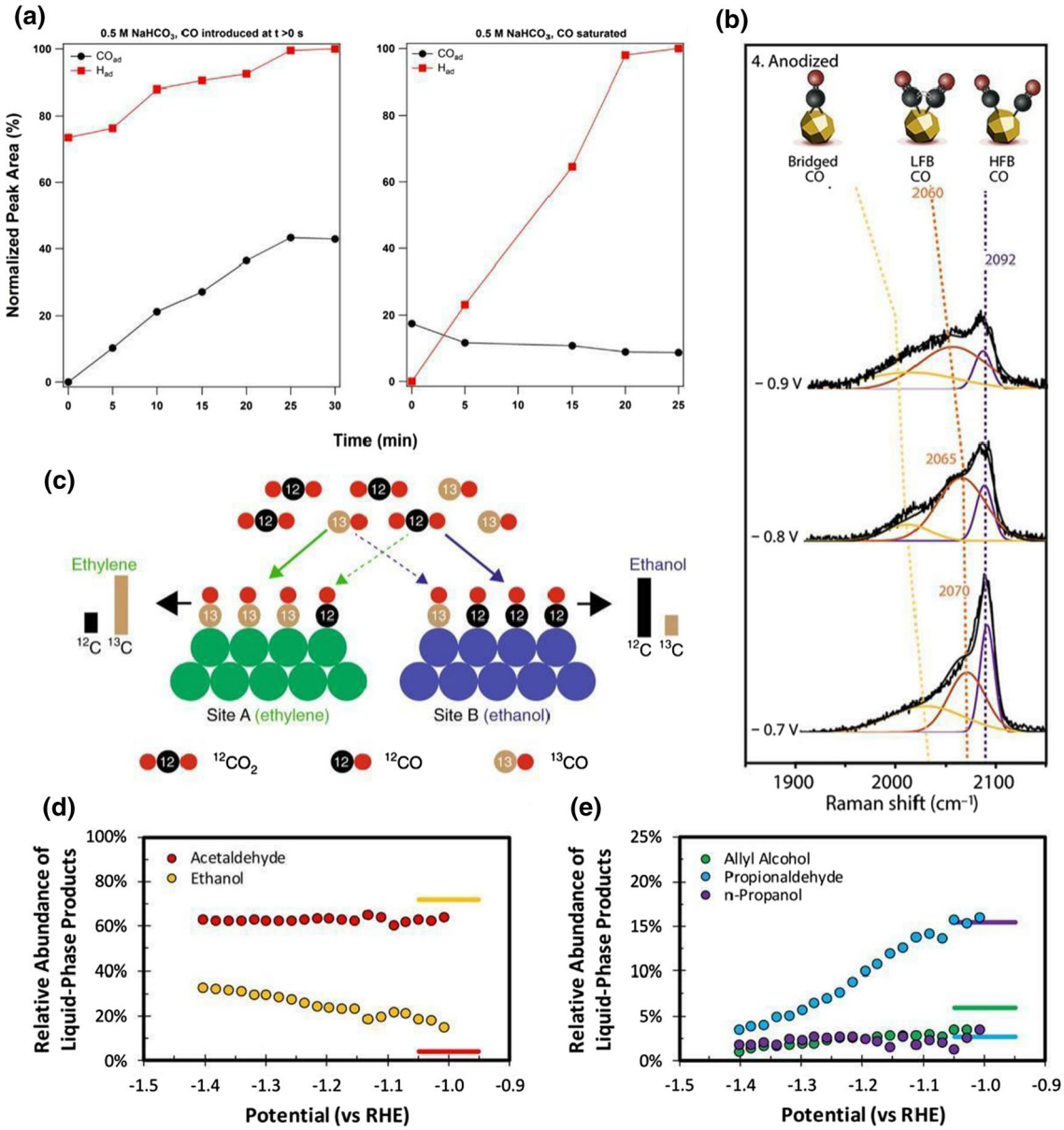

Fig. 14 In situ intermediate characterization techniques. **a** Time-resolved surface-enhanced infrared absorption spectroscopy (SEIRA)-integrated peak areas for *CO and *H bands after peak deconvolution, reported as a percentage of the largest *H peak. CO introduced on the H-saturated Cu surface (left). *H accumulation on a CO-saturated Cu surface (right). Reproduced with permission from Ref. [56]. Copyright 2016 American Chemical Society. **b** Comparison of the steady-state Raman spectra during reduction at various potentials. Reproduced with permission from Ref. [101]. Copyright 2021 Wiley–VCH. **c** Hypothetical scenario for the reduction in a mixture of ^{13}CO and $^{12}CO_2$. Reproduced with permission from Ref. [172]. Copyright 2019 Springer Nature. **d, e** MS signal of the relative abundance of the liquid phase products generated on Cu. The solid lines represent the relative abundances of the liquid phase products in a traditional H-cell when analyzing the bulk electrolyte. Reproduced with permission from Ref. [61]. Copyright 2018 American Chemical Society

For the precise quantification of different isotopic atoms, nuclear magnetic resonance and MS are usually applied in the isotopic analysis. Ma et al. [111] reported that fluorine-modified Cu promotes the activation of water supported by a drastically reduced KIE of H/D (H/D is defined as the ratio of the rate of ethylene formation in H_2O and D_2O), and a KIE value close to 1 indicates that dissociation of H_2O is no longer involved in the RDS. Ager and coworkers [172] used $^{12}CO_2/^{13}CO$ co-feed experiments to identify three product-specific active sites on OD-Cu electrocatalysts; these three sites lead to the production of ethylene, ethanol or acetate, and *n*-propanol (Fig. 14c). Chang et al. [62] elucidated the

formation mechanism of the C_3 products by combining isotopic labeling with in situ spectroscopy. Since only 36% of *n*-propanol is derived from the cross-coupling of CO with acetaldehyde, the adsorbed methylcarbonyl intermediate is proposed to be the bifurcation point of the reaction pathway for the C_2 and C_3 products.

In situ MS is typically used to achieve the real-time detection and semiquantification of gaseous and evaporable liquid products based on mass-to-charge ratios. By improving the time resolution of in situ MS, the formation of intermediates and products under transient operation can be detected, and the potential correlations between them can be established [173, 174]. Koper and coworkers [54] proposed two possible reaction mechanisms for ethylene formation using online electrochemical MS. In one pathway, C_2H_4 shares an intermediate with CH_4 on the Cu (111) and Cu (100) surfaces, while in the other pathway, the selective reduction of CO to C_2H_4 occurs on Cu (100) at a relatively low overpotential, presumably via the formation of a CO dimer. Clark et al. [61] found that the ratio of aldehydes to alcohols detected in the region close to the Cu electrode was much higher than that in the bulk electrolyte. With increasing overpotential, the relative abundance of ethanol rises along with a decrease in propionaldehyde, suggesting that acetaldehyde is a bifurcated intermediate for ethanol and propionaldehyde formation, while *n*-propanol is formed via propionaldehyde (Fig. 14d, e).

Summary and Perspectives

This review focuses on strategies to improve the selectivity of CO_2RR to C_{2+} products through manipulation of the intermediates on the surface of the Cu-based catalysts. A systematic discussion of C_{2+} formation mechanisms revealed that the binding energies and competitive adsorption of intermediates on the catalyst surface are crucial for C_{2+} selectivity as these factors can affect the C–C coupling and hydrodeoxygenation processes. Subsequently, we provided deep insights into the manipulating strategies and factors influencing intermediate adsorption, covering topics such as surface structural effects, introduction of additional elements, chemical state effects, electric field effects, substrate effects, confinement effects, and local microenvironment effects. Table 1 summarizes the electrochemical CO_2-to-C_{2+} performance of Cu-based electrocatalysts according to the intermediate manipulation strategies. Through an optimal combination of these strategies, C_{2+} production can be further improved in practical applications. For example, the simultaneous utilization of doping and confinement strategies improves the selectivity of C_{2+} products without any catalytic activity degradation [107]. Specifically, quasigraphitic C shells can stabilize the crystal size of Cu nanoparticles based on the confinement effects, while doping with *p*-block elements can drastically improve the C_{2+} selectivity and cathodic power conversion efficiency via the modulation of the binding properties of the Cu catalysts.

As the CO_2RR involves complex reaction steps and numerous intermediates, the use of advanced in situ characterization techniques is important for elucidating the relationship among structures, intermediates, and performance. In particular, the *operando* characterization of intermediates is the key to accurately revealing the reaction pathways and RDS of the CO_2RR, and thus, such studies can provide useful guidance for optimizing catalysts. Therefore, we comprehensively discussed various in situ characterization techniques to identify the intermediates and their adsorption states under operating conditions. These techniques included IR spectroscopy, Raman spectroscopy, MS, and quantitative isotope measurements. In addition, theoretical calculations and simulations that closely match the actual operating conditions are also irreplaceable critical tools for understanding the catalytic mechanisms in detail. By considering the adsorption intermediate as a bridge, the correlation between the catalyst structure and catalytic performance was established to promote the practical application of CO_2RR.

Although the activity and selectivity of CO_2 reduction to C_{2+} products on Cu-based catalysts have greatly improved in recent years, their in-depth mechanisms are still unclear, and the industrial application of the CO_2RR is still challenging. On the one hand, most reaction mechanisms for the conversion of CO_2 to C_{2+} products are presumed based on the final product distribution. Such an inference from the effect to the cause makes it difficult to objectively and accurately understand the actual reaction process. On the other hand, for meeting the industrial requirements for the CO_2RR, the focus is on greatly reducing the cost of the catalytic systems rather than further improving catalyst selectivity, activity, and stability. Note that cofeeding of CO_2 with other feedstocks provides a promising pathway for the generation of high-value-added products, and this pathway should be actively explored. To this end, efforts should be focused on the following aspects in future research:

1) Clarification of the CO_2RR mechanisms. A combination of in situ experimental evidence and theoretical calculations can provide insights into the actual reaction pathways of the CO_2RR, thus directing the rational design of catalysts. In particular, experimental observations can provide modeling guidance for theoretical calculations, in turn enabling the high-throughput screening of highly active catalysts with intermediates with suitable binding energies [176]. To enable the precise customization of active sites on Cu-based catalysts, there is an urgent need to develop high temporal and spatial resolu-

Table 1 Summary of electrochemical CO_2-to-C_{2+} performance for various Cu-based catalysts. The stability time marked "MEA" indicates that the stability test of the electrocatalyst was performed in a membrane electrode assembly

Strategy	Electrocatalyst	Cell configuration	Electrolyte	E (V vs. RHE)	j (mA/cm^2)	FE_{C2+} (%)	Main C_{2+} product	Stability time (h)	Ref
Facet	Cu-CO_2	Flow cell	1 mol/L KOH	−0.71	577	90	67% C_2H_4	65 (MEA)	[80]
	Cu (100)-rich films	Flow cell	2 mol/L KOH	−0.85	150	87	59% C_2H_4	4.5	[65]
	100-cycled Cu	H-cell	0.25 mol/L $KHCO_3$	−0.96	68	61	32% C_2H_4	2	[23]
Defect	Nano-defective Cu NS	H-cell	0.1 mol/L K_2SO_4	−1.18	60	83	83% C_2H_4	14	[17]
	Cu_KBr (60 s)	H-cell	0.1 mol/L $KHCO_3$	−1.15	43	72	49% C_2H_4	–	[85]
Grain boundary	Cu_3N-derived Cu NWs	H-cell	0.1 mol/L $KHCO_3$	−1.0	57	86	66% C_2H_4	28	[100]
	CuO-Fast cold	Flow cell	1 mol/L KOH	−1.0	300	76	36% C_2H_4	–	[96]
	GB-Cu NP	Flow cell	1 mol/L KOH	−1.0	60	73	38% C_2H_4	–	[97]
Vacancy	Cu_2S-Cu-V	Flow cell	1 mol/L KOH	−0.92	400	56	25% C_2H_5OH	16	[104]
	CuS_x-DSV	H-cell	0.1 mol/L $KHCO_3$	−1.05	20	18	15% C_3H_7OH	10	[21]
Doping	Cu (N)@ quasi-graphitic C	Flow cell	1 mol/L KOH	−0.69	400	82	71% C_2H_4	180 (MEA)	[107]
	F-Cu	Flow cell	0.75 mol/L KOH	−0.98	1,600	80	65% C_2H_4	40	[111]
	$Ce(OH)_x$/Cu	Flow cell	1 mol/L KOH	−0.7	300	80	43% C_2H_5OH	6	[19]
	Cu(B)	H-cell	0.1 mol/L $KHCO_3$	−1.1	70	79	52% C_2H_4	40	[37]
Alloy	Cu-Al alloys	Flow cell	1 mol/L KOH	−1.5	400	90	80% C_2H_4	100	[123]
	CuAg wire	Flow cell	1 mol/L KOH	−0.7	300	85	60% C_2H_4	–	[58]
Electric field	Cu-PTFE-99 NN	Flow cell	1 mol/L KOH	−0.76	300	85	45% C_2H_4	25	[138]
	Mesoporous Cu nanoribbons	Flow cell	1 mol/L KOH	−1.23	423	82	50% C_2H_4	10	[135]
Substrate	Graphite/C NPs/Cu/PTFE	Flow cell	7 mol/L KOH	−0.55	250	84	70% C_2H_4	150	[16]
	N-Nanodiamond /Cu	H-cell	0.5 mol/L $KHCO_3$	−0.5	1	64	35% CH_3COO^-	120	[142]
Confinement	N–C/Cu	Flow cell	1 mol/L KOH	−0.68	300	93	52% C_2H_5OH	15 (MEA)	[20]
	Cu/$HMCS_5$-20%	Flow cell	1 mol/L KOH	−1.0	275	89	69% C_2H_4	20	[175]
	3-shell HoMSs Cu	Flow cell	0.5 mol/L $KHCO_3$	−0.88	668	77	32% C_2H_4	8	[151]

tion characterization techniques to accurately detect the intermediates [177, 178].

2) Rational design of electrolyzers. Recently, it was established that high-efficiency gas diffusion electrodes and membrane electrode assembly are more promising electrolytic devices for the industrial application of the CO_2RR [179]. The optimization of electrolyzers can not only reduce the working voltage, but also significantly increase the current density (by up to 1.6 A/cm^2), which is close to the technoeconomic requirements for the industrial application of CO_2RR [111, 180]. However, the problems of flooding and salt precipitation that occur at gas diffusion electrodes over long-term electrolysis should be addressed to avoid a rapid decrease in selectivity and current density. Moreover, the formation and crossover of carbonates in alkaline electrolytes also affects the single-pass conversion of CO_2 and contaminates the O_2 stream released from anodes, thereby

increasing the cost of feedstock and separation. Impressively, the solid-electrolyte reactor, which decouples the ion conduction and product collection, successfully recovers the substantial carbon loss that occurs during CO_2RR electrolysis and avoids the requirement for cost-intensive downstream product-separation processes [181–183]. Besides, acid electrolytes [184] and pulsed electrolysis [185] were also used to avoid carbonate accumulation, offering promising ways to realize long-term electrolysis.

3) Cofeeding of CO_2 and other reactants. Currently, high-purity CO_2, which requires considerable energy to capture and purify, is the main feedstock used in experimental research. However, because of its high cost, high-purity CO_2 is impractical for industrial applications of CO_2RRs. In this situation, cofeeding CO_2 with other chemicals can decrease the cost of CO_2 purification and/or create high-value products, in turn improving the technical economy of the catalytic systems. For example, flue gas is a potential source of CO_2 and can be adopted to reduce the purification cost; however, more deliberate catalyst design and pressurization are required to overcome the competition reaction caused by the oxidizing gases [186, 187]. Besides, the formation of C–N compounds by the coelectrolysis of CO_2 and nitrogen-containing reactants also holds great promise [188–190]. For example, the coactivation of N_2 and CO_2 enables the electrosynthesis of desirable urea [191].

In conclusion, the CO_2RR provides a promising solution for converting CO_2 emissions into valuable feedstocks. Encouragingly, much progress has been achieved toward the electroreduction of CO_2 to C_{2+} products using Cu-based catalysts during the last decades. However, many problems still persist for industrial applications. Together with a mechanistic exploration supported by advanced in situ characterization techniques and theoretical simulations, the optimization of electrolyzers and CO_2 feeding modes is expected to further advance the industrial applications of the CO_2RR.

Acknowledgements We gratefully appreciate the support of the National Natural Science Foundation of China (Nos. 51972223, 51932005 and 22109116), the Natural Science Foundation of Tianjin (No. 20JCYBJC01550), the Fundamental Research Funds for the Central Universities, and the Haihe Laboratory of Sustainable Chemical Transformations.

Declarations

Conflict of interest The authors declare that there is no conflict of interest.

References

1. Ling YF, Ma QL, Yu YF et al (2021) Optimization strategies for selective CO_2 electroreduction to fuels. Trans Tianjin Univ 27(3):180–200
2. Li L, Li XD, Sun YF et al (2022) Rational design of electrocatalytic carbon dioxide reduction for a zero-carbon network. Chem Soc Rev 51(4):1234–1252
3. Mallapaty S (2020) How China could be carbon neutral by mid-century. Nature 586(7830):482–483
4. Hepburn C, Adlen E, Beddington J et al (2019) The technological and economic prospects for CO_2 utilization and removal. Nature 575(7781):87–97
5. De Luna P, Hahn C, Higgins D et al (2019) What would it take for renewably powered electrosynthesis to displace petrochemical processes? Science 364(6438): eaav3506
6. Endrődi B, Kecsenovity E, Samu A et al (2020) High carbonate ion conductance of a robust PiperION membrane allows industrial current density and conversion in a zero-gap carbon dioxide electrolyzer cell. Energy Environ Sci 13(11):4098–4105
7. Ren SX, Joulié D, Salvatore D et al (2019) Molecular electrocatalysts can mediate fast, selective CO_2 reduction in a flow cell. Science 365(6451):367–369
8. Jiao JQ, Lin R, Liu SJ et al (2019) Copper atom-pair catalyst anchored on alloy nanowires for selective and efficient electrochemical reduction of CO_2. Nat Chem 11(3):222–228
9. Zhao Y, Liu XL, Chen DC et al (2021) Atomic-level-designed copper atoms on hierarchically porous gold architectures for high-efficiency electrochemical CO_2 reduction. Sci China Mater 64(8):1900–1909
10. Li JC, Kuang Y, Meng YT et al (2020) Electroreduction of CO_2 to formate on a copper-based electrocatalyst at high pressures with high energy conversion efficiency. J Am Chem Soc 142(16):7276–7282
11. Fan L, Xia C, Zhu P et al (2020) Electrochemical CO_2 reduction to high-concentration pure formic acid solutions in an all-solid-state reactor. Nat Commun 11:3633
12. Weng Z, Wu YS, Wang MY et al (2018) Active sites of copper-complex catalytic materials for electrochemical carbon dioxide reduction. Nat Commun 9:415
13. Zhu HL, Huang JR, Zhang XW et al (2021) Highly efficient electroconversion of CO_2 into CH_4 by a metal-organic framework with trigonal pyramidal $Cu(I)N_3$ active sites. ACS Catal 11(18):11786–11792
14. Zhang L, Li XX, Lang ZL et al (2021) Enhanced cuprophilic interactions in crystalline catalysts facilitate the highly selective electroreduction of CO_2 to CH_4. J Am Chem Soc 143(10):3808–3816
15. García de Arquer FP, Dinh CT, Ozden A et al (2020) CO_2 electrolysis to multicarbon products at activities greater than 1 A/cm^2. Science 367(6478):661–666

16. Dinh CT, Burdyny T, Kibria MG et al (2018) CO_2 electroreduction to ethylene via hydroxide-mediated copper catalysis at an abrupt interface. Science 360(6390):783–787
17. Zhang BX, Zhang JL, Hua ML et al (2020) Highly electrocatalytic ethylene production from CO_2 on nanodefective Cu nanosheets. J Am Chem Soc 142(31):13606–13613
18. Li YC, Wang ZY, Yuan TG et al (2019) Binding site diversity promotes CO_2 electroreduction to ethanol. J Am Chem Soc 141(21):8584–8591
19. Luo MC, Wang ZY, Li YC et al (2019) Hydroxide promotes carbon dioxide electroreduction to ethanol on copper via tuning of adsorbed hydrogen. Nat Commun 10:5814
20. Wang X, Wang ZY, García de Arquer FP et al (2020) Efficient electrically powered CO_2-to-ethanol via suppression of deoxygenation. Nat Energy 5(6):478–486
21. Peng C, Luo G, Zhang JB et al (2021) Double sulfur vacancies by lithium tuning enhance CO_2 electroreduction to n-propanol. Nat Commun 12:1580
22. Tang MT, Peng HJ, Stenlid JH et al (2021) Exploring trends on coupling mechanisms toward C_3 product formation in $CO_{(2)}R$. J Phys Chem C 125(48):26437–26447
23. Jiang K, Sandberg RB, Akey AJ et al (2018) Metal ion cycling of Cu foil for selective C-C coupling in electrochemical CO_2 reduction. Nat Catal 1(2):111–119
24. Bushuyev OS, de Luna P, Dinh CT et al (2018) What should we make with CO_2 and how can we make it? Joule 2(5):825–832
25. Fan L, Xia C, Yang FQ et al (2020) Strategies in catalysts and electrolyzer design for electrochemical CO_2 reduction toward C_{2+} products. Sci Adv 6(8): eaay3111
26. Bagger A, Ju W, Varela AS et al (2017) Electrochemical CO_2 reduction: a classification problem. ChemPhysChem 18(22):3266–3273
27. Kuhl KP, Cave ER, Abram DN et al (2012) New insights into the electrochemical reduction of carbon dioxide on metallic copper surfaces. Energy Environ Sci 5(5):7050–7059
28. Ross MB, de Luna P, Li YF et al (2019) Designing materials for electrochemical carbon dioxide recycling. Nat Catal 2(8):648–658
29. Ma WC, He XY, Wang W et al (2021) Electrocatalytic reduction of CO_2 and CO to multi-carbon compounds over Cu-based catalysts. Chem Soc Rev 50(23):12897–12914
30. Birdja YY, Pérez-Gallent E, Figueiredo MC et al (2019) Advances and challenges in understanding the electrocatalytic conversion of carbon dioxide to fuels. Nat Energy 4(9):732–745
31. Zhang YJ, Sethuraman V, Michalsky R et al (2014) Competition between CO_2 reduction and H_2 evolution on transition-metal electrocatalysts. ACS Catal 4(10):3742–3748
32. Kortlever R, Shen J, Schouten KJP et al (2015) Catalysts and reaction pathways for the electrochemical reduction of carbon dioxide. J Phys Chem Lett 6(20):4073–4082
33. Zhi X, Vasileff A, Zheng Y et al (2021) Role of oxygen-bound reaction intermediates in selective electrochemical CO_2 reduction. Energy Environ Sci 14(7):3912–3930
34. Mariano RG, Kang M, Wahab OJ et al (2021) Microstructural origin of locally enhanced CO_2 electroreduction activity on gold. Nat Mater 20(7):1000–1006
35. Verdaguer-Casadevall A, Li CW, Johansson TP et al (2015) Probing the active surface sites for CO reduction on oxide-derived copper electrocatalysts. J Am Chem Soc 137(31):9808–9811
36. Mariano RG, McKelvey K, White HS et al (2017) Selective increase in CO_2 electroreduction activity at grain-boundary surface terminations. Science 358(6367):1187–1192
37. Zhou YS, Che FL, Liu M et al (2018) Dopant-induced electron localization drives CO_2 reduction to C_2 hydrocarbons. Nat Chem 10(9):974–980
38. Xiang KS, Liu YC, Li CF et al (2021) Microenvironmental feeding and stabilization of C_2H_4 intermediates by iodide-doped copper nanowire arrays to boost C_2H_6 formation. Energy Fuels 35(19):15987–15994
39. Han ZS, Han DL, Chen Z et al (2022) Steering surface reconstruction of copper with electrolyte additives for CO_2 electroreduction. Nat Commun 13:3158
40. Monteiro MCO, Dattila F, Hagedoorn B et al (2021) Absence of CO_2 electroreduction on copper, gold and silver electrodes without metal cations in solution. Nat Catal 4(8):654–662
41. Hori Y, Wakebe H, Tsukamoto T et al (1994) Electrocatalytic process of CO selectivity in electrochemical reduction of CO_2 at metal electrodes in aqueous media. Electrochim Acta 39(11–12):1833–1839
42. Hori Y, Takahashi I, Koga O et al (2003) Electrochemical reduction of carbon dioxide at various series of copper single crystal electrodes. J Mol Catal A Chem 199(1–2):39–47
43. Shi C, Hansen HA, Lausche AC et al (2014) Trends in electrochemical CO_2 reduction activity for open and close-packed metal surfaces. Phys Chem Chem Phys 16(10):4720–4727
44. Nitopi S, Bertheussen E, Scott SB et al (2019) Progress and perspectives of electrochemical CO_2 reduction on copper in aqueous electrolyte. Chem Rev 119(12):7610–7672
45. Wang L, Nitopi SA, Bertheussen E et al (2018) Electrochemical carbon monoxide reduction on polycrystalline copper: effects of potential, pressure, and pH on selectivity toward multicarbon and oxygenated products. ACS Catal 8(8):7445–7454
46. Zhong DZ, Zhao ZJ, Zhao Q et al (2021) Coupling of Cu(100) and (110) facets promotes carbon dioxide conversion to hydrocarbons and alcohols. Angew Chem Int Ed Engl 60(9):4879–4885
47. Sandberg RB, Montoya JH, Chan KR et al (2016) CO-CO coupling on Cu facets:coverage, strain and field effects. Surf Sci 654:56–62
48. Jeong HM, Kwon Y, Won JH et al (2020) Atomic-scale spacing between copper facets for the electrochemical reduction of carbon dioxide. Adv Energy Mater 10(10):1903423
49. Luo WJ, Nie XW, Janik MJ et al (2016) Facet dependence of CO_2 reduction paths on Cu electrodes. ACS Catal 6(1):219–229
50. de Luna P, Quintero-Bermudez R, Dinh CT et al (2018) Catalyst electro-redeposition controls morphology and oxidation state for selective carbon dioxide reduction. Nat Catal 1(2):103–110
51. Wang X, Ou PF, Ozden A et al (2022) Efficient electrosynthesis of n-propanol from carbon monoxide using a Ag–Ru–Cu catalyst. Nat Energy 7(2):170–176
52. Li J, Chang K, Zhang HC et al (2019) Effectively increased efficiency for electroreduction of carbon monoxide using supported polycrystalline copper powder electrocatalysts. ACS Catal 9(6):4709–4718
53. Santatiwongchai J, Faungnawakij K, Hirunsit P (2021) Comprehensive mechanism of CO_2 electroreduction toward ethylene and ethanol: the solvent effect from explicit water-Cu(100) interface models. ACS Catal 11(15):9688–9701
54. Schouten KJP, Qin ZS, Pérez Gallent E et al (2012) Two pathways for the formation of ethylene in CO reduction on single-crystal copper electrodes. J Am Chem Soc 134(24):9864–9867
55. Chang XX, Li J, Xiong HC et al (2022) C-C coupling is unlikely to be the rate-determining step in the formation of C_{2+} products in the copper-catalyzed electrochemical reduction of CO. Angew Chem Int Ed Engl 61(2):e202111167
56. Heyes J, Dunwell M, Xu BJ (2016) CO_2 reduction on Cu at low overpotentials with surface-enhanced in situ spectroscopy. J Phys Chem C 120(31):17334–17341
57. Cheng T, Xiao H, Goddard WA (2017) Full atomistic reaction mechanism with kinetics for CO reduction on Cu(100) from

ab initio molecular dynamics free-energy calculations at 298 K. Proc Natl Acad Sci USA 114(8):1795–1800
58. Hoang TT, Verma S, Ma SC et al (2018) Nanoporous copper-silver alloys by additive-controlled electrodeposition for the selective electroreduction of CO_2 to ethylene and ethanol. J Am Chem Soc 140(17):5791–5797
59. Wang X, Wang ZY, Zhuang TT et al (2019) Efficient upgrading of CO to C_3 fuel using asymmetric C−C coupling active sites. Nat Commun 10:5186
60. Hori Y, Takahashi R, Yoshinami Y et al (1997) Electrochemical reduction of CO at a copper electrode. J Phys Chem B 101(36):7075–7081
61. Clark EL, Bell AT (2018) Direct observation of the local reaction environment during the electrochemical reduction of CO_2. J Am Chem Soc 140(22):7012–7020
62. Chang XX, Malkani A, Yang X et al (2020) Mechanistic insights into electroreductive C−C coupling between CO and acetaldehyde into multicarbon products. J Am Chem Soc 142(6):2975–2983
63. Veenstra FLP, Ackerl N, Martín AJ et al (2020) Laser-microstructured copper reveals selectivity patterns in the electrocatalytic reduction of CO_2. Chem 6(7):1707–1722
64. de Gregorio GL, Burdyny T, Loiudice A et al (2020) Facet-dependent selectivity of Cu catalysts in electrochemical CO_2 reduction at commercially viable current densities. ACS Catal 10(9):4854–4862
65. Zhang G, Zhao ZJ, Cheng DF et al (2021) Efficient CO_2 electroreduction on facet-selective copper films with high conversion rate. Nat Commun 12:5745
66. Chang CC, Ku MS (2021) Role of high-index facet Cu(711) surface in controlling the C2 selectivity for CO_2 reduction reaction—a DFT study. J Phys Chem C 125(20):10919–10925
67. Hahn C, Hatsukade T, Kim YG et al (2017) Engineering Cu surfaces for the electrocatalytic conversion of CO_2: controlling selectivity toward oxygenates and hydrocarbons. Proc Natl Acad Sci USA 114(23):5918–5923
68. Chen Y, Fan ZX, Wang J et al (2020) Ethylene selectivity in electrocatalytic CO_2 reduction on Cu nanomaterials: a crystal phase-dependent study. J Am Chem Soc 142(29):12760–12766. https://doi.org/10.1021/jacs.0c04981
69. Liu JZ, Guo L (2021) In situ self-reconstruction inducing amorphous species:a key to electrocatalysis. Matter 4(9):2850–2873
70. Weng Z, Zhang X, Wu YS et al (2017) Self-cleaning catalyst electrodes for stabilized CO_2 reduction to hydrocarbons. Angew Chem Int Ed Engl 56(42):13135–13139
71. Lee SH, Lin JC, Farmand M et al (2021) Oxidation state and surface reconstruction of Cu under CO_2 reduction conditions from *in situ* X-ray characterization. J Am Chem Soc 143(2):588–592
72. Zhu CY, Zhao SW, Shi GS et al (2022) Structure-function correlation and dynamic restructuring of Cu for highly efficient electrochemical CO_2 conversion. Chemsuschem 15(7):e202200068
73. Chen JY, Wang L (2022) Effects of the catalyst dynamic changes and influence of the reaction environment on the performance of electrochemical CO_2 reduction. Adv Mater 34(25):e2103900
74. Raaijman SJ, Arulmozhi N, Koper MTM (2021) Morphological stability of copper surfaces under reducing conditions. ACS Appl Mater Interfaces 13(41):48730–48744
75. Arán-Ais RM, Rizo R, Grosse P et al (2020) Imaging electrochemically synthesized Cu_2O cubes and their morphological evolution under conditions relevant to CO_2 electroreduction. Nat Commun 11:3489
76. Simon GH, Kley CS, Roldan Cuenya B (2021) Potential-dependent morphology of copper catalysts during CO_2 electroreduction revealed by in situ atomic force microscopy. Angew Chem Int Ed Engl 60(5):2561–2568
77. Kim YG, Baricuatro JH, Javier A et al (2014) The evolution of the polycrystalline copper surface, first to Cu(111) and then to Cu(100), at a fixed CO_2RR potential: a study by *operando* EC-STM. Langmuir 30(50):15053–15056
78. Kim YG, Baricuatro JH, Soriaga MP (2018) Surface reconstruction of polycrystalline Cu electrodes in aqueous $KHCO_3$ electrolyte at potentials in the early stages of CO_2 reduction. Electrocatalysis 9(4):526–530
79. Wang HX, Liang Z, Tang M et al (2019) Self-selective catalyst synthesis for CO_2 reduction. Joule 3(8):1927–1936
80. Wang YH, Wang ZY, Dinh CT et al (2020) Catalyst synthesis under CO_2 electroreduction favours faceting and promotes renewable fuels electrosynthesis. Nat Catal 3(2):98–106
81. Kim JY, Park W, Choi C et al (2021) High facets on nanowrinkled Cu via chemical vapor deposition graphene growth for efficient CO_2 reduction into ethanol. ACS Catal 11(9):5658–5665
82. Vollmer S, Witte G, Wöll C (2001) Determination of site specific adsorption energies of CO on copper. Catal Lett 77(1–3):97–101
83. Li J, Che FL, Pang YJ et al (2018) Copper adparticle enabled selective electrosynthesis of n-propanol. Nat Commun 9:4614
84. Piqué O, Low QH, Handoko AD et al (2021) Selectivity map for the late stages of CO and CO_2 reduction to C_2 species on copper electrodes. Angew Chem Int Ed Engl 60(19):10784–10790
85. Kim T, Palmore GTR (2020) A scalable method for preparing Cu electrocatalysts that convert CO_2 into C_{2+} products. Nat Commun 11:3622
86. Jiang K, Huang YF, Zeng GS et al (2020) Effects of surface roughness on the electrochemical reduction of CO_2 over Cu. ACS Energy Lett 5(4):1206–1214
87. Loiudice A, Lobaccaro P, Kamali EA et al (2016) Tailoring copper nanocrystals towards C_2 products in electrochemical CO_2 reduction. Angew Chem Int Ed Engl 55(19):5789–5792
88. Handoko AD, Ong CW, Huang Y et al (2016) Mechanistic insights into the selective electroreduction of carbon dioxide to ethylene on Cu_2O-derived copper catalysts. J Phys Chem C 120(36):20058–20067
89. Reske R, Mistry H, Behafarid F et al (2014) Particle size effects in the catalytic electroreduction of CO_2 on Cu nanoparticles. J Am Chem Soc 136(19):6978–6986
90. Rong WF, Zou HY, Zang WJ et al (2021) Size-dependent activity and selectivity of atomic-level copper nanoclusters during CO/CO_2 electroreduction. Angew Chem Int Ed Engl 60(1):466–472
91. Li CW, Kanan MW (2012) CO_2 reduction at low overpotential on Cu electrodes resulting from the reduction of thick Cu_2O films. J Am Chem Soc 134(17):7231–7234
92. Li CW, Ciston J, Kanan MW (2014) Electroreduction of carbon monoxide to liquid fuel on oxide-derived nanocrystalline copper. Nature 508(7497):504–507
93. Feng XF, Jiang KL, Fan SS et al (2016) A direct grain-boundary-activity correlation for CO electroreduction on Cu nanoparticles. ACS Cent Sci 2(3):169–174
94. Chen CJ, Yan XP, Wu YH et al (2021) The *in situ* study of surface species and structures of oxide-derived copper catalysts for electrochemical CO_2 reduction. Chem Sci 12(16):5938–5943
95. Chen CJ, Sun XF, Yan XP et al (2020) A strategy to control the grain boundary density and Cu^+/Cu^0 ratio of Cu-based catalysts for efficient electroreduction of CO_2 to C_2 products. Green Chem 22(5):1572–1576
96. Yang C, Shen HC, Guan AX et al (2020) Fast cooling induced grain-boundary-rich copper oxide for electrocatalytic carbon dioxide reduction to ethanol. J Colloid Interface Sci 570:375–381
97. Chen ZQ, Wang T, Liu B et al (2020) Grain-boundary-rich copper for efficient solar-driven electrochemical CO_2 reduction to ethylene and ethanol. J Am Chem Soc 142(15):6878–6883

98. Sun H, Chen L, Xiong LK et al (2021) Promoting ethylene production over a wide potential window on Cu crystallites induced and stabilized via current shock and charge delocalization. Nat Commun 12:6823
99. Cheng DF, Zhao ZJ, Zhang G et al (2021) The nature of active sites for carbon dioxide electroreduction over oxide-derived copper catalysts. Nat Commun 12:395
100. Mi YY, Shen SB, Peng XY et al (2019) Selective electroreduction of CO_2 to C2 products over Cu_3N-derived Cu nanowires. ChemElectroChem 6(9):2393–2397
101. An HY, Wu LF, Mandemaker LDB et al (2021) Sub-second time-resolved surface-enhanced Raman spectroscopy reveals dynamic CO intermediates during electrochemical CO_2 reduction on copper. Angew Chem Int Ed Engl 60(30):16576–16584
102. Kim Y, Park S, Shin SJ et al (2020) Time-resolved observation of C−C coupling intermediates on Cu electrodes for selective electrochemical CO_2 reduction. Energy Environ Sci 13(11):4301–4311
103. Pang YJ, Li J, Wang ZY et al (2019) Efficient electrocatalytic conversion of carbon monoxide to propanol using fragmented copper. Nat Catal 2(3):251–258
104. Zhuang TT, Liang ZQ, Seifitokaldani A et al (2018) Steering post-C–C coupling selectivity enables high efficiency electroreduction of carbon dioxide to multi-carbon alcohols. Nat Catal 1(6):421–428
105. Wang SS, Ding PC, Li Z et al (2021) Subsurface-carbon-induced local charge of copper for an on-surface displacement reaction. Angew Chem Int Ed 60(43):23123–23127
106. Li MH, Ma YY, Chen J et al (2021) Residual chlorine induced cationic active species on a porous copper electrocatalyst for highly stable electrochemical CO_2 reduction to C_{2+}. Angew Chem Int Ed Engl 60(20):11487–11493
107. Kim JY, Hong D, Lee JC et al (2021) Quasi-graphitic carbon shell-induced Cu confinement promotes electrocatalytic CO_2 reduction toward C_{2+} products. Nat Commun 12:3765
108. Zhi X, Jiao Y, Zheng Y et al (2021) Directing the selectivity of CO_2 electroreduction to target C_2 products *via* non-metal doping on Cu surfaces. J Mater Chem A 9(10):6345–6351
109. Song YF, Junqueira JRC, Sikdar N et al (2021) B-Cu-Zn gas diffusion electrodes for CO_2 electroreduction to C_{2+} products at high current densities. Angew Chem Int Ed Engl 60(16):9135–9141
110. Chen CJ, Sun XF, Lu L et al (2018) Efficient electroreduction of CO_2 to C_2 products over B-doped oxide-derived copper. Green Chem 20(20):4579–4583
111. Ma WC, Xie SJ, Liu TT et al (2020) Electrocatalytic reduction of CO_2 to ethylene and ethanol through hydrogen-assisted C-C coupling over fluorine-modified copper. Nat Catal 3(6):478–487
112. Chen RZ, Cheng L, Liu JZ et al (2022) Toward high-performance CO_2-to-C_2 electroreduction via linker tuning on MOF-derived catalysts. Small 18(18):2200720
113. Clark EL, Hahn C, Jaramillo TF et al (2017) Electrochemical CO_2 reduction over compressively strained CuAg surface alloys with enhanced multi-carbon oxygenate selectivity. J Am Chem Soc 139(44):15848–15857
114. Xiao H, Cheng T, Goddard WA (2017) Atomistic mechanisms underlying selectivities in C_1 and C_2 products from electrochemical reduction of CO on Cu(111). J Am Chem Soc 139(1):130–136
115. Lum Y, Cheng T, Goddard WA et al (2018) Electrochemical CO reduction builds solvent water into oxygenate products. J Am Chem Soc 140(30):9337–9340
116. Li J, Xu AN, Li FW et al (2020) Enhanced multi-carbon alcohol electroproduction from CO via modulated hydrogen adsorption. Nat Commun 11:3685
117. He JF, Johnson NJJ, Huang AX et al (2018) Electrocatalytic alloys for CO_2 reduction. Chemsuschem 11(1):48–57
118. Hitt JL, Li YC, Tao SS et al (2021) A high throughput optical method for studying compositional effects in electrocatalysts for CO_2 reduction. Nat Commun 12:1114
119. Weitzner SE, Akhade SA, Kashi AR et al (2021) Evaluating the stability and activity of dilute Cu-based alloys for electrochemical CO_2 reduction. J Chem Phys 155(11):114702
120. Xu YZ, Li CL, Xiao YQ et al (2022) Tuning the selectivity of liquid products of CO_2RR by Cu-Ag alloying. ACS Appl Mater Interfaces 14(9):11567–11574
121. Hu F, Yang L, Jiang YW et al (2021) Ultrastable Cu catalyst for CO_2 electroreduction to multicarbon liquid fuels by tuning C−C coupling with CuTi subsurface. Angew Chem Int Ed 60(50):26122–26127
122. Li YL, Tian ZQ, Chen L (2021) Theoretical understanding of the interface effect in promoting electrochemical CO_2 reduction on Cu-Pd alloys. J Phys Chem C 125(39):21381–21389
123. Zhong M, Tran K, Min YM et al (2020) Accelerated discovery of CO_2 electrocatalysts using active machine learning. Nature 581(7807):178–183
124. Kim C, Cho KM, Park K et al (2021) Cu/Cu_2O interconnected porous aerogel catalyst for highly productive electrosynthesis of ethanol from CO_2. Adv Funct Mater 31(32):2102142
125. Lum Y, Ager JW (2018) Stability of residual oxides in oxide-derived copper catalysts for electrochemical CO_2 reduction investigated with ^{18}O labeling. Angew Chem Int Ed 57(2):551–554
126. Lei Q, Zhu H, Song KP et al (2020) Investigating the origin of enhanced C_{2+} selectivity in oxide-/hydroxide-derived copper electrodes during CO_2 electroreduction. J Am Chem Soc 142(9):4213–4222
127. Mandal L, Yang KR, Motapothula MR et al (2018) Investigating the role of copper oxide in electrochemical CO_2 reduction in real time. ACS Appl Mater Interfaces 10(10):8574–8584
128. Cavalca F, Ferragut R, Aghion S et al (2017) Nature and distribution of stable subsurface oxygen in copper electrodes during electrochemical CO_2 reduction. J Phys Chem C 121(45):25003–25009
129. Mistry H, Varela AS, Bonifacio CS et al (2016) Highly selective plasma-activated copper catalysts for carbon dioxide reduction to ethylene. Nat Commun 7:12123
130. Yang PP, Zhang XL, Gao FY et al (2020) Protecting copper oxidation state via intermediate confinement for selective CO_2 electroreduction to C_{2+} fuels. J Am Chem Soc 142(13):6400–6408
131. Chou TC, Chang CC, Yu HL et al (2020) Controlling the oxidation state of the Cu electrode and reaction intermediates for electrochemical CO_2 reduction to ethylene. J Am Chem Soc 142(6):2857–2867
132. Xiao H, Goddard WA, Cheng T et al (2017) Cu metal embedded in oxidized matrix catalyst to promote CO_2 activation and CO dimerization for electrochemical reduction of CO_2. Proc Natl Acad Sci USA 114(26):6685–6688
133. Liu M, Pang YJ, Zhang B et al (2016) Enhanced electrocatalytic CO_2 reduction via field-induced reagent concentration. Nature 537(7620):382–386
134. Jiang HJ, Hou ZH, Luo Y (2017) Unraveling the mechanism for the sharp-tip enhanced electrocatalytic carbon dioxide reduction: the kinetics decide. Angew Chem Int Ed 56(49):15617–15621
135. Huo H, Wang J, Fan QK et al (2021) Cu-MOFs derived porous Cu nanoribbons with strengthened electric field for selective CO_2 electroreduction to C_{2+} fuels. Adv Energy Mater 11(42):2102447
136. Li H, Zhou HM, Zhou YJ et al (2022) Electric-field promoted C−C coupling over Cu nanoneedles for CO_2 electroreduction to C_2 products. Chin J Catal 43(2):519–525

137. Zhou YJ, Liang YQ, Fu JW et al (2022) Vertical Cu nanoneedle arrays enhance the local electric field promoting C_2 hydrocarbons in the CO_2 electroreduction. Nano Lett 22(5):1963–1970
138. Yang BP, Liu K, Li H et al (2022) Accelerating CO_2 electroreduction to multicarbon products via synergistic electric-thermal field on copper nanoneedles. J Am Chem Soc 144(7):3039–3049
139. An PD, Wei L, Li H et al (2020) Enhancing CO_2 reduction by suppressing hydrogen evolution with polytetrafluoroethylene protected copper nanoneedles. J Mater Chem A 8(31):15936–15941
140. Suominen M, Kallio T (2021) What we currently know about carbon-supported metal and metal oxide nanomaterials in electrochemical CO_2 reduction. ChemElectroChem 8(13):2397–2406
141. Zhang JG, Guo YT, Shang B et al (2021) Unveiling the synergistic effect between graphitic carbon nitride and Cu_2O toward CO_2 electroreduction to C_2H_4. Chemsuschem 14(3):929–937
142. Wang HX, Tzeng YK, Ji YF et al (2020) Synergistic enhancement of electrocatalytic CO_2 reduction to C_2 oxygenates at nitrogen-doped nanodiamonds/Cu interface. Nat Nanotechnol 15(2):131–137
143. Song Y, Peng R, Hensley DK et al (2016) High-selectivity electrochemical conversion of CO_2 to ethanol using a copper nanoparticle/N-doped graphene electrode. ChemistrySelect 1(19):6055–6061
144. Grosse P, Gao DF, Scholten F et al (2018) Dynamic changes in the structure, chemical state and catalytic selectivity of Cu nanocubes during CO_2 electroreduction: size and support effects. Angew Chem Int Ed 57(21):6192–6197
145. Möller T, Scholten F, Thanh TN et al (2020) Electrocatalytic CO_2 reduction on CuO_x nanocubes: tracking the evolution of chemical state, geometric structure, and catalytic selectivity using *operando* spectroscopy. Angew Chem Int Ed 59(41):17974–17983
146. Jaugstetter M, Blanc N, Kratz M et al (2022) Electrochemistry under confinement. Chem Soc Rev 51(7):2491–2543
147. Pang YJ, Burdyny T, Dinh CT et al (2017) Joint tuning of nanostructured Cu-oxide morphology and local electrolyte programs high-rate CO_2 reduction to C_2H_4. Green Chem 19(17):4023–4030
148. Yang KD, Ko WR, Lee JH et al (2017) Morphology-directed selective production of ethylene or ethane from CO_2 on a Cu mesopore electrode. Angew Chem Int Ed Engl 56(3):796–800
149. Zhuang TT, Pang YJ, Liang ZQ et al (2018) Copper nanocavities confine intermediates for efficient electrosynthesis of C3 alcohol fuels from carbon monoxide. Nat Catal 1(12):946–951
150. Liu B, Cai C, Yang BP et al (2021) Intermediate enrichment effect of porous Cu catalyst for CO_2 electroreduction to C_2 fuels. Electrochim Acta 388:138552
151. Liu CX, Zhang ML, Li JW et al (2022) Nanoconfinement engineering over hollow multi-shell structured copper towards efficient electrocatalytical C−C coupling. Angew Chem Int Ed Engl 61(3):e202113498
152. Tan DX, Zhang JL, Yao L et al (2020) Multi-shelled CuO microboxes for carbon dioxide reduction to ethylene. Nano Res 13(3):768–774
153. Junqueira JRC, O'Mara PB, Wilde P et al (2021) Combining nanoconfinement in Ag core/porous Cu shell nanoparticles with gas diffusion electrodes for improved electrocatalytic carbon dioxide reduction. ChemElectroChem 8(24):4848–4853
154. Zhong YZ, Kong XD, Song ZM et al (2022) Adjusting local CO confinement in porous-shell Ag@Cu catalysts for enhancing C−C coupling toward CO_2 eletroreduction. Nano Lett 22(6):2554–2560
155. Bui JC, Kim C, King AJ et al (2022) Engineering catalyst-electrolyte microenvironments to optimize the activity and selectivity for the electrochemical reduction of CO_2 on Cu and Ag. Acc Chem Res 55(4):484–494
156. Gupta N, Gattrell M, MacDougall B (2006) Calculation for the cathode surface concentrations in the electrochemical reduction of CO_2 in $KHCO_3$ solutions. J Appl Electrochem 36(2):161–172
157. Henckel DA, Counihan MJ, Holmes HE et al (2021) Potential dependence of the local pH in a CO_2 reduction electrolyzer. ACS Catal 11(1):255–263
158. Moradzaman M, Mul G (2021) Optimizing CO coverage on rough copper electrodes: effect of the partial pressure of CO and electrolyte anions (pH) on selectivity toward ethylene. J Phys Chem C 125(12):6546–6554
159. Lu X, Zhu CQ, Wu ZS et al (2020) *In situ* observation of the pH gradient near the gas diffusion electrode of CO_2 reduction in alkaline electrolyte. J Am Chem Soc 142(36):15438–15444
160. Hori Y, Murata A, Takahashi R (1989) Formation of hydrocarbons in the electrochemical reduction of carbon dioxide at a copper electrode in aqueous solution. J Chem Soc Faraday Trans 85(8):2309–2326
161. Resasco J, Lum Y, Clark E et al (2018) Effects of anion identity and concentration on electrochemical reduction of CO_2. ChemElectroChem 5(7):1064–1072
162. Resasco J, Chen LD, Clark E et al (2017) Promoter effects of alkali metal cations on the electrochemical reduction of carbon dioxide. J Am Chem Soc 139(32):11277–11287
163. Liu HJ, Qi ZM, Song L (2021) *In situ* electrocatalytic infrared spectroscopy for dynamic reactions. J Phys Chem C 125(44):24289–24300
164. Hori Y, Koga O, Yamazaki H et al (1995) Infrared spectroscopy of adsorbed CO and intermediate species in electrochemical reduction of CO_2 to hydrocarbons on a Cu electrode. Electrochim Acta 40(16):2617–2622
165. Moradzaman M, Mul G (2020) Infrared analysis of interfacial phenomena during electrochemical reduction of CO_2 over polycrystalline copper electrodes. ACS Catal 10(15):8049–8057. https://doi.org/10.1021/acscatal.0c02130
166. Pérez-Gallent E, Figueiredo MC, Calle-Vallejo F et al (2017) Spectroscopic observation of a hydrogenated CO dimer intermediate during CO reduction on Cu(100) electrodes. Angew Chem Int Ed 56(13):3621–3624
167. Kurouski D, Dazzi A, Zenobi R et al (2020) Infrared and Raman chemical imaging and spectroscopy at the nanoscale. Chem Soc Rev 49(11):3315–3347
168. Jiang S, Klingan K, Pasquini C et al (2018) New aspects of *operando* Raman spectroscopy applied to electrochemical CO_2 reduction on Cu foams. J Chem Phys 150(4):041718
169. Gao J, Zhang H, Guo XY et al (2019) Selective C−C coupling in carbon dioxide electroreduction via efficient spillover of intermediates as supported by *operando* Raman spectroscopy. J Am Chem Soc 141(47):18704–18714
170. Zhan C, Dattila F, Rettenmaier C et al (2021) Revealing the CO coverage-driven C-C coupling mechanism for electrochemical CO_2 reduction on Cu_2O nanocubes *via operando* Raman spectroscopy. ACS Catal 11(13):7694–7701
171. Lin YH, Deng CY, Wu L et al (2020) Quantitative isotope measurements in heterogeneous photocatalysis and electrocatalysis. Energy Environ Sci 13(9):2602–2617
172. Lum Y, Ager JW (2019) Evidence for product-specific active sites on oxide-derived Cu catalysts for electrochemical CO_2 reduction. Nat Catal 2(1):86–93
173. Khanipour P, Löffler M, Reichert AM et al (2019) Electrochemical real-time mass spectrometry (EC-RTMS): monitoring electrochemical reaction products in real time. Angew Chem Int Ed Engl 58(22):7273–7277
174. Ye K, Zhang GR, Ma XY et al (2022) Resolving local reaction environment toward an optimized CO_2-to-CO conversion performance. Energy Environ Sci 15(2):749–759

175. Pan Y, Li HD, Xiong J et al (2022) Protecting the state of Cu clusters and nanoconfinement engineering over hollow mesoporous carbon spheres for electrocatalytical C-C coupling. Appl Catal B Environ 306:121111
176. Zhang N, Yang BP, Liu K et al (2021) Machine learning in screening high performance electrocatalysts for CO_2 reduction. Small Methods 5(11):e2100987
177. Zhu CY, Zhang ZB, Zhong LX et al (2021) Product-specific active site motifs of Cu for electrochemical CO_2 reduction. Chem 7(2):406–420
178. Guo SX, Bentley CL, Kang M et al (2022) Advanced spatiotemporal voltammetric techniques for kinetic analysis and active site determination in the electrochemical reduction of CO_2. Acc Chem Res 55(3):241–251
179. Wakerley D, Lamaison S, Wicks J et al (2022) Gas diffusion electrodes, reactor designs and key metrics of low-temperature CO_2 electrolysers. Nat Energy 7(2):130–143
180. Kibria MG, Edwards JP, Gabardo CM et al (2019) Electrochemical CO_2 reduction into chemical feedstocks: from mechanistic electrocatalysis models to system design. Adv Mater 31(31):1807166
181. Xia C, Zhu P, Jiang Q et al (2019) Continuous production of pure liquid fuel solutions via electrocatalytic CO_2 reduction using solid-electrolyte devices. Nat Energy 4(9):776–785
182. Zhu P, Wang HT (2021) High-purity and high-concentration liquid fuels through CO_2 electroreduction. Nat Catal 4(11):943–951
183. Kim JY, Zhu P, Chen FY et al (2022) Recovering carbon losses in CO_2 electrolysis using a solid electrolyte reactor. Nat Catal 5(4):288–299
184. Huang JE, Li FW, Ozden A et al (2021) CO_2 electrolysis to multicarbon products in strong acid. Science 372(6546):1074–1078
185. Xu Y, Edwards JP, Liu SJ et al (2021) Self-cleaning CO_2 reduction systems: unsteady electrochemical forcing enables stability. ACS Energy Lett 6(2):809–815
186. Cheng YY, Hou J, Kang P (2021) Integrated capture and electroreduction of flue gas CO_2 to formate using amine functionalized SnO_x nanoparticles. ACS Energy Lett 6(9):3352–3358
187. Xu Y, Edwards JP, Zhong JJ et al (2020) Oxygen-tolerant electroproduction of C_2 products from simulated flue gas. Energy Environ Sci 13(2):554–561
188. Li JN, Kornienko N (2022) Electrochemically driven C-N bond formation from CO_2 and ammonia at the triple-phase boundary. Chem Sci 13(14):3957–3964
189. Tao ZX, Rooney CL, Liang YY et al (2021) Accessing organonitrogen compounds via C-N coupling in electrocatalytic CO_2 reduction. J Am Chem Soc 143(47):19630–19642
190. Rooney CL, Wu YS, Tao ZX et al (2021) Electrochemical reductive N-methylation with CO_2 enabled by a molecular catalyst. J Am Chem Soc 143(47):19983–19991
191. Yuan ML, Chen JW, Xu Y et al (2021) Highly selective electroreduction of N_2 and CO_2 to urea over artificial frustrated Lewis pairs. Energy Environ Sci 14(12):6605–6615

Zhe Weng is a full professor at the School of Chemical Engineering and Technology, Tianjin University. He received his Ph.D. in Materials Science and Engineering from University of Chinese Academy of Sciences in 2013. His research interests concern on electrode materials and electrolytes for electrochemical energy storage (multivalent rechargeable batteries) and electrocatalytic energy conversion (carbon dioxide/nitrogen/nitrate electroreduction).